

APPLICATIONS IN BROADBAND THz SPECTROSCOPY
TOWARDS
MATERIAL STUDIES

A THESIS SUBMITTED TO
THE GRADUATE SCHOOL OF NATURAL AND APPLIED SCIENCES
OF
MIDDLE EAST TECHNICAL UNIVERSITY

BY

ZEYNEP TÜRKŞEN

IN PARTIAL FULFILLMENT OF THE REQUIREMENTS
FOR
THE DEGREE OF MASTER OF SCIENCE
IN
PHYSICS

JANUARY 2011

Approval of the Thesis:

**APPLICATIONS IN BROADBAND THZ SPECTROSCOPY TOWARDS
MATERIAL STUDIES**

Submitted by **ZEYNEP TÜRKŞEN** in partial fulfillment of the requirements for the degree of **Master of Science in Physics Department, Middle East Technical University** by,

Prof. Dr. Canan Özgen _____
Dean, Graduate School of **Natural and Applied Sciences**

Prof. Dr. Sinan Bilikmen _____
Head of Department, **Physics**

Assist. Prof. Dr. Hakan Altan _____
Supervisor, **Physics Dept., METU**

Examining Committee Members:

Prof. Dr. Sinan Bilikmen _____
Physics Dept., METU

Assist. Prof. Dr. Hakan Altan _____
Physics Dept., METU

Prof. Dr. Mehmet Parlak _____
Physics Dept., METU

Assist. Prof. Dr. Behzat Şahin _____
Electrical and Electronics Engineering Dept., METU

Dr. Halil Berberoğlu _____
Physics Dept., METU

Date: _____

I hereby declare that all information in this document has been obtained and presented in accordance with academic rules and ethical conduct. I also declare that, as required by these rules and conduct, I have fully cited and referenced all material and results that are not original to this work.

Name, Last Name: Zeynep TÜRKŞEN

Signature:

ABSTRACT

APPLICATIONS IN BROADBAND THz SPECTROSCOPY TOWARDS MATERIAL STUDIES

Türkşen, Zeynep

M.Sc. Department of Physics

Supervisor: Assist. Prof. Dr. Hakan Altan

January 2011, 65 pages

The purpose of this work was to construct and analyze a THz time domain spectroscopy (THz-TDS) system by using a nanojoule energy per pulse ultrafast laser (non-amplified ultrafast laser or oscillator) source and a non-linear optical generation method for THz generation. First a THz-TDS system, which uses photoconductive antenna (PCA) method for THz generation, was built to understand the working principles of these types of systems. This THz-TDS system which used PCA for generation and a 2mm thick <110> ZnTe crystal for detection had a bandwidth up to 1 THz with a 1000:1 signal to noise ratio (S/N). Using this system, various materials were investigated to study the usefulness of the obtained bandwidth. Absorption coefficient and refractive indices of the sample materials were calculated. Results showed that the bandwidth of the system was not sufficient to obtain fingerprint

properties of these materials. In order to improve the system, optical rectification method was used for THz generation. A different THz-TDS system was built with a 1mm thick <110> ZnTe crystal used for the method of non-linear generation of THz radiation. Theoretical calculations of radiated intensity and electric field were done to analyze the expected bandwidth of the system. Results showed that the generation and the detection crystal thicknesses affect the obtained bandwidth of the system in that the bandwidth limiting factor is the crystal thickness and not the ultrafast laser pulse duration. Especially for detection, measurements obtained with both a 1mm thick and 2mm thick <110> ZnTe crystal showed that there was not much difference in bandwidth as was predicted by theory. Also in order to increase the signal to noise ratio, the optics used in the system were optimized. It was found that by using same focal lengths for focusing and collimating optics around the generation crystal and by using a short focal length parabolic mirror, S/N could be improved. After these improvements this THz-TDS system which uses optical rectification for THz generation and electro-optic method for THz detection had a larger bandwidth up to 3 THz but with a lower 100:1 signal to noise ratio.

Keywords: THz-TDS, terahertz, crystal generation, optical rectification, signal to noise ratio

ÖZ

GENİŞ BANTLI THz SPEKTROSKOPİSİNİN MADDELER ÜZERİNDEKİ UYGULAMALARI

Türkşen, Zeynep
Yüksek Lisans, Fizik Bölümü
Tez Yöneticisi: Yrd. Doç. Dr. Hakan Altan

Ocak 2011, 65 sayfa

Bu çalışmanın amacı, THz üretimi için atım başına nanojul enerjiye sahip ultra hızlı lazer (osilator için yükseltilmemiş ultra hızlı lazer) kaynağı kullanarak zamana dayalı THz spektroskopi (THz-TDS) sistemi kurmak ve incelemektir. Öncelikle bu tür sistemlerin çalışma prensiplerini anlamak için, fotoiletken anten (PCA) metodu kullanan bir THz-TDS sistemi kurulmuştur. Üretim için PCA ve algılama için 2 mm kalınlığında <110> kesimli ZnTe kristali kullanan bu sistem, 1 THz'e kadar bant genişliğine ve 1000:1 sinyal gürültü oranına (S/N) sahiptir. Elde edilen bant genişliğinin kullanılabilirliğini öğrenmek için, bu sistem kullanılarak çeşitli maddeler incelenmiştir. Örnek maddelerin soğurma katsayısı ve kırılma indisi hesaplanmıştır. Sonuçlar şunu göstermiştir; sistemin bant genişliği bu maddelerin parmak izi özelliklerini elde etmek için yeterli değildir. Sistemi geliştirmek için THz üretimi için optiksel doğrultma yöntemi kullanılmıştır. Doğrusal olmayan THz üretim yöntemi için 1 mm kalınlığında ve <110> kesimli ZnTe kristali kullanılarak farklı bir

THz-TDS sistemi kurulmuştur. Beklenen bant genişliğini incelemek için, yayılan radyasyonun şiddeti ve elektrik alanı teorik olarak hesaplanmıştır. Sonuçlar, üretim ve algılama kristal kalınlıklarının sistemde elde edilen bant genişliğini etkilediğini ve bant genişliğini limitleyen faktörün ultra hızlı lazerin atım süresi değil kristal kalınlığı olduğunu göstermiştir. Özellikle algılamada, 1mm ve 2 mm kalınlığa sahip <110> kesimli ZnTe kristalleri ile alınan ölçümlerin sonuçları teoride öngörüldüğü gibi bant genişliğinde fazla değişim göstermemektedir. Ayrıca, sinyal gürültü oranını arttırmak için sistemde kullanılan optikler iyileştirilmiştir. Odaklama ve toplama için aynı odak uzaklığına sahip optikler ve kısa odak uzaklığına sahip parabolik ayna kullanıldığında S/N oranının artırılabilirdiği görülmüştür. Bu iyileştirmelerden sonra üretim için optiksel doğrultma ve algılama için electro-optik yöntemini kullanan bu THz-TDS sistemi daha geniş bir bant genişliği olan 3 THz'e kadar çıkmış fakat daha düşük olan 100:1 sinyal gürültü oranına sahip olmuştur.

Anahtar kelime: THz spektroskopisi, terahertz, kristal üretim, optiksel doğrultma, sinyal gürültü oranı

To my family

ACKNOWLEDGMENT

I would like to thank to my supervisor Assist. Prof. Dr. Hakan Altan for his advice, guidance and criticism. He also gave me the opportunity to work in his research group. Also I would like to thank to the rest of my thesis committee; Prof. Dr. Sinan Bilikmen, Prof. Dr. Mehmet Parlak, Assist. Prof. Dr. Behzat Şahin and Dr. Halil Berberoğlu.

I would like to thank to all of my colleagues Can Koral and Seda Kayra for their help. I would also like to thank my former colleagues Zahite Tosun and Gülten Karaođlan for sharing their experiences with me. Specially thanks to Seda for her support and friendship. I would also like to thank to Gökhan Alkaç for his analytical and mathematical intelligence and infinite patience.

I would like to express my deepest gratitude to my sister, Sibel Selçuk. Nothing would be easy without her. Especially, I would like to thank Olgu for his patience, encouragement, endless support and love.

TABLE OF CONTENTS

ABSTRACT	iv
ÖZ	vi
TABLE OF CONTENTS	ix
LIST OF TABLES	xii
LIST OF FIGURES	xiii
CHAPTERS	
1. INTRODUCTION	1
1.1 THz GENERATION	3
1.2 THz DETECTION	4
2. THz TIME DOMAIN SPECTROSCOPY	6
2.1 THz SPECTROSCOPY	6
2.2 THz IMAGING	7
2.3 GENERATION OF THz RADIATION	8
2.3.1 Photoconductive Antenna Method for Generation	10
2.3.2 Optical Rectification for Generation	11
2.4 DETECTION OF THz RADIATION	13
2.4.1 Photoconductive Antenna Method for Detection	14
2.4.2 Electro-Optic (EO) Sampling	15

3. THz TIME DOMAIN SPECTROMETER WITH PHOTOCONDUCTIVE ANTENNA GENERATION	16
3.1 SYSTEM OVERVIEW	17
3.1.1 Detailed Description of the Spectrometer	17
3.1.2 Data Collection	23
3.2 THEORY AND ANALYSIS	26
3.3 FOCUSING OF THz RADIATION ON SMALL SAMPLES.....	28
3.4 EXAMPLE MEASUREMENTS	34
3.5 DISCUSSION	38
4. THz TIME DOMAIN SPECTROMETER WITH CRYSTAL GENERATION	39
4.1 SYSTEM INFORMATION.....	39
4.2 CRYSTAL GENERATION	41
4.2.1 Why ZnTe Crystal?	42
4.2.2 Generation with ZnTe Crystal.....	44
4.3 CRYSTAL DETECTION.....	52
4.4 RESULTS OF CRYSTAL - CRYSTAL THz SYSTEM	55
5. CONCLUSION	58
REFERENCES.....	61

LIST OF TABLES

TABLES

Table 2.1 Summary for pulse and CW THz radiation techniques	9
Table 3.1 Electrical and Optical excitation parameters for PCA	22
Table 3.2 Table of spot size and confocal parameter relations	31
Table 3.3 Specifications of the samples	35
Table 4.1 THz peak values with different lens of changing focal length	55
Table 4.2 Comparison of the power spectrum for the different crystal-crystal systems	56
Table 4.3 Comparison of the power spectrum for different OAPM Focal Length	57

LIST OF FIGURES

FIGURES

Figure 1.1 Electromagnetic Spectrum.....	1
Figure 2.1 a) Side view of PC antenna b) Top view of PC antenna	10
Figure 3.1 Schematic representation of the system.....	19
Figure 3.2 Dimensions of the PCA 44-06-10-001 (units are in micrometers) [17] ...	20
Figure 3.3 Photographs of PC antenna.....	21
a. Front view (laser side) b. Back view (THz side) [17].....	21
Figure 3.4 Temporal waveform of THz radiation measured with THz-TDS	25
Figure 3.5 Power spectrum of the temporal waveform shown in Figure 3.4.....	26
Figure 3.6 THz-TDS system with THz focusing lenses	30
Figure 3.7 Spot size and confocal parameters.....	31
Figure 3.8 Temporal waveform of THz radiation collected by THz-TDS system with focusing lenses.....	33
Figure 3.9 Power spectrum of the temporal waveform shown in Figure 3.8.....	34
Figure 3.10 Sample Analysis of Selenium1	36
a. Absorption Coefficient b. Refractive index	36
Figure 3.11 Sample Analysis of Selenium2.....	36
a. Absorption Coefficient b. Refractive index	36
Figure 3.12 Sample Analysis of White Selenium	37
a. Absorption Coefficient b. Refractive index	37

Figure 3.13 Sample Analysis of Vitamin B	37
a. Absorption Coefficient b. Refractive index	37
Figure 4.2 Optical Group Refractive Index.....	43
Figure 4.3 THz Refractive Index	43
Figure 4.4 Walk-off length of ZnTe crystal	44
Figure 4.5 Crystal Orientation according to the incoming electric field (E_0)	52
Figure 4.6 Coherent length of ZnTe crystal.	53
Figure 4.7 Schematic representation of EO crystal detection	54

CHAPTER 1

INTRODUCTION

Terahertz (THz) is a frequency unit, which corresponds to 10^{12} hertz in the spectrum. In Physics, Terahertz is also known as the electromagnetic (EM) radiation where the propagating frequencies are in the THz range which is between 10^{11} to 10^{13} hertz. In the EM spectrum this frequency range corresponds to the region between Microwave and Infrared Region, as seen in Figure 1.1. The waves from this radiation are called T-ray and the radiation is called T-ray radiation. At 1 THz frequency, the photon energy is 4.1 meV, the temperature is 48 K, the period is 1 ps, the wavelength is 300 μm and the wave number is 33.3 cm^{-1} [1].

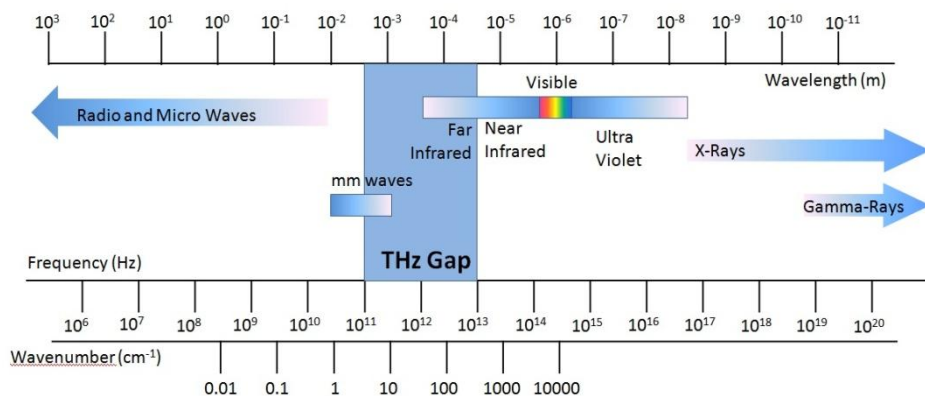


Figure 1.1 Electromagnetic Spectrum

The unit conversions mentioned in the above paragraph clearly show that THz region has a unique place in the spectrum. Within this portion of the spectrum, THz radiation has several applications, as different ranges of the spectrum have its own unique spectroscopic properties. In the electromagnetic spectrum, the Microwave region is considered to have applications in electronics and the far infrared region is considered to have applications in optics. Therefore THz frequencies are considered to fall between electronics and optics [2]. In order to generate or to detect THz radiation both technologies are necessary. Historically in the field of Terahertz physics combining optics and electronics was the biggest challenge. This is often attributed to the differences in the principles of optics and electronics. That is why this part of the spectrum is also known as “THz Gap” [1].

Although the THz radiation is not visible, it can be detected by electrical or optical techniques. THz radiation is not only naturally occurring but also emitted from THz sources. However, naturally occurring THz radiation is not easy to use in THz systems due to its incoherence [3]. The T-rays can be classified in two types. One of which is pulsed radiation and the other one is continuous wave (CW) radiation [4]. These two types of radiations have different applications in the field of physics, chemistry, biology, and material science [5].

Unique properties of the T-rays make this area appealing to scientists. Even though it requires high technology and is high-priced to set up a THz system, the unrevealed portion of the spectrum draws attention to this area and the information obtained makes it worthwhile. One of the areas of interest is the polarity of materials. THz is sensitive to dipole structures. Polar molecules show high absorption in this frequency region. THz absorption spectra help to determine rotational and vibrational properties of highly absorptive materials. Since these properties are specific for every material, the THz region is known for having fingerprints of many materials [2]. A second area of interest is ionization of materials; T-rays have low photon energy, which leads to non-ionization. One advantage of this is; THz radiation is safe for human beings and also nondestructive for the samples which are analyzed under THz radiation [6]. Also high water absorption of THz makes it difficult to penetrate deep into skin. A third area of interest is optical properties of materials, T-rays have a

longer wavelength which provides less effect from Mie scattering [3]. Last of all, materials have different optical properties in THz region. Some materials are opaque at THz frequencies like metals which are highly reflective. Examples of transparent materials at THz frequencies are glass and water. There are also some materials which are transmissive in this region, i.e., polymers (Teflon, TPX etc.), dielectrics (plastics, paper, clothes, wood etc.) and semiconductors (silicon, germanium, gallium arsenide, quartz etc.). Based on the properties of these various materials, they can be used to construct THz systems. [1].

1.1 THz GENERATION

The technology required to obtain THz radiation goes back to the 1960s. The development of laser technology had a tremendous affect on the THz field [4]. The development of mode-lock lasers in mid 1970s and the use of photoconductive (PC) material for switching as antennas was the starting point for PC generation. First, Auston and Lee introduced the PC switching in the 1980s. Then, Mourou et al. [9] and Heidemann et al. [10] developed the switching to produce antennas [3]. Soon after, PC antenna structure was improved by Smith, Auston, and Nuss in 1988 and this was the first published paper generating THz frequencies using mode-locked lasers [4]. The PC antennas continued to improve in structure and began to be used extensively in THz systems. In 1989 Van Exter, Fattinger, and Grischkowsky showed that the with these structures, these systems can be used as spectroscopic tools [12]. CW THz generation was also done with PC antenna structures, their use termed as photomixers, in 1993 by Brown et al. [13].

Another THz generation technique, as old as PC generation, is optical rectification. Optical part of the spectrum played a great role on this generation. Optical rectification originated in 1960s [14]. In the early 1970s generation of EM radiation in far-infrared region emerged, where an optical technique with a non-linear crystal and a mode-lock laser was used. This was published by two research groups: Yajima

et al. [15] and Yang et al. in 1971 [16]. This can be considered as the beginning of this technique for THz generation, since some of the far-infrared region overlaps with the THz gap.

PC antenna and optical rectification are the oldest but still the most popular techniques for THz pulse generation. Other than these methods, in 1990s Zhang and coworkers studied on a subpicosecond EM generation from semiconductor surfaces [17]. Hu et al. contributed these studies by changing the temperature of the semiconductors [18]. Around the same time, the observation of the radiation from charge oscillations in semiconductor quantum structures drew some attention. Leo et al. reported the first work on this topic and observed the first THz radiation from asymmetric coupled quantum wells [19]. Later in 1994 quantum cascade laser (QCL) was developed by Bell Laboratories which is a continuing and promising new technology [20].

In 1995 different studies on generation of THz with semiconductors were conducted. THz emission from coherent infrared-active photons in a semiconductor was first observed by Dekorsy et al. [21], then THz radiation from cold plasma oscillations in a semiconductor reported by Kersting et al. which was followed by Gornik's group's findings [22]. Hangyo et al. studied high- T_c superconducting thin-film bridge and THz emission from this structure [23].

1.2 THz DETECTION

THz generation with PC antenna and optical rectification were the first but they are the most frequently used methods. The reversed processes of each technique were also used for THz detection. In 1980s Auston and coworkers developed these techniques. First, in 1983 Auston et al. started sampling radiation-damaged Si-on-sapphire (RD-SOS) with PC film in the millimeter range [24]. Then, 1.6 ps radiation was detected with PC switching by Auston, Cheung and Smith in 1984 [25]. In the

same year, Auston et al. also used electro-optic (EO) sampling technique for detection of THz [26].

Methods for the generation and detection of THz radiation played a significant role for the applications of THz radiation. At the time not only the THz generation but also the THz applications were a developing field in Physics. Applications of THz radiation can be basically divided into two main topics: spectroscopy and imaging. All of the THz radiation types can be used for both of these applications, however pulsed radiation is most frequently used for spectroscopy and CW radiation is used mostly for imaging.

In this study we compare both photoconductive and optical rectification methods of THz generation and try to focus on developing a THz system driven by nanojoule energy per pulse ultrafast laser (non-amplified laser) source that uses both optical rectification for generation as well as the linear electro-optic effect for detection. We give special attention to the issue of signal to noise of such a system and discuss methods to improve the signal to noise ratio by careful selection of THz optics. In Chapter 2 we give a brief explanation of THz-Time Domain Spectroscopy. In the next chapter, our experimental setup based on THz generated by a PC antenna and detected by electro-optic detection is explained. In the fourth chapter we discuss the development of a THz-TDS system driven by a nanojoule energy per pulse ultrafast laser (non-amplified laser) source where the THz pulse is generated by optical rectification and detection is done again with electro-optic method. The generated THz intensity and electric field of such a system is derived for the methods and materials used in this work. In the last chapter the work of this thesis is summarized.

CHAPTER 2

THz TIME DOMAIN SPECTROSCOPY

To date spectroscopy is the most common technique used to understand the molecular structures of materials. Initial studies of spectroscopy go back to 1920s. First spectroscopic work in the submillimeter wave region was published by Czerny showing rotational spectra of HCl in 1925, which was accepted as the beginning of infra-red molecular spectroscopy [9]. However, spectroscopic work in the THz region began in the 1990s.

2.1 THz SPECTROSCOPY

THz spectroscopy is mainly separated into three sections; Terahertz time-domain spectroscopy (THz-TDS), time resolved terahertz spectroscopy (TRTS) and terahertz emission spectroscopy (TES) [28].

THz-TDS is basically probing THz wave in the time-domain. In a THz pulse system, both generation and detection occurs in the same system. The system uses an ultrafast laser pulse, which is divided into two optical beams in the system. One generates THz pulse, which is called pump beam; the other detects the pulse, which is called probe beam. Probe beam explores amplitude of the THz pulse over time. Thus, THz waveform is obtained as a function of time. This waveform can be used as reference waveform. A sample placed under THz radiation to be probed in the

system and a waveform is obtained, which is called sample waveform. By comparing the two waveforms under Fourier Transform, spectroscopic information can be obtained.

THz-TDS can be compared with the other spectroscopic techniques which are performed in the frequency domain, such as FTIR. Since THz-TDS uses coherent detection, it can measure both amplitude and phase of the electric field of the THz pulse, where as FTIR can only measure intensity. With the information obtained absorption coefficient and the refractive index of the sample can be calculated. In addition to that, complex permittivity calculations can be obtained without Kramers-Kronig analysis. The temporal resolution of THz-TDS is in the order of ps, thus have a higher resolution than FTIR which is considered as another advantage [3].

TRTS is a time dependent THz spectroscopy which uses photo excitation on the sample. This excitation is mostly done by a laser pulse and with the help of this photo excitation the change in the carriers and the change in the permittivity of the sample can be investigated. Main difference from the THz-TDS is that TRTS measures the dynamic properties of the material.

TES is another spectroscopic technique which uses the sample under investigation as a THz emitter to determine the THz pulse shape. By this technique information about the motion of high energy photo excited carriers are obtained [28]. Pump-probe systems consider the evolution of energy; however TES investigates velocity and momentum changes.

2.2 THz IMAGING

THz-TDS systems can also be used for imaging applications. THz-TDS is an active imaging method which means the radiation source is an external source [3]. THz radiation is generated in the system and used or either for transmission or for reflection geometries in the system. By focusing THz pulse on the target sample the terahertz waveform can be obtained. By positioning the sample on the x-y stage the

focusing point on the sample can be changed. On each point a waveform can be measured and by combining these waveforms the image of the target sample can be acquired pixel by pixel. Waveforms differ at each point by amplitude or time delay. Image formed by using amplitude gives the absorbance of the THz pulse within the sample. On the other hand with time delay in between the waveforms, one can obtain the variations in the thickness of the sample as well as a three dimensional profile [29]. Including spectral information to the image helps to detect differences at certain locations of the sample. This technique mainly supports security applications [20].

THz imaging using pulsed THz systems started in 1995 at Bell Laboratories. Hu and Nuss demonstrated the first image by pulsed THz imaging system [31].

2.3 GENERATION OF THZ RADIATION

Based on the wave generation, THz radiation can be divided into two groups. One is pulsed wave generation the other is continuous wave (CW) generation. In this thesis two different techniques of THz pulse generation will be considered. Broadband THz generation can be obtained either from a nonlinear media (optical rectification) or from accelerating electrons (PC Antenna). Various crystals are used as a common nonlinear media. Accelerating electrons can be formed either in a photoconductive antenna or by an electron accelerator.

CW THz radiation can also be generated from nonlinear crystals as well as from photoconductive antenna. Another way of generating the radiation is the use of free-electron lasers (or gas lasers). In the Table 2.1 the generation techniques for pulsed and CW THz radiation is summarized.

The techniques which were used in this thesis will be briefly explained in the following sections.

Table 2.1 Summary for pulse and CW THz radiation techniques [1, 4, 32, 33]

	Generation Technique	Generated Material/Medium
Pulsed THz Radiation	Optical Rectification	Dielectrics, Semiconductors, Organic Materials
	Transient Photoconductive Switching	Photoconductive Antenna
	Emission from Periodically undulated electron beam	Electron Accelerators
	Surge Current (Surface Depletion Field)	Semiconductor Surface
	Tunneling of Electron Wave Packet	Quantum Semiconductor Structures
	Coherent Longitudinal Optical Phonons	Semiconductors, Semimetals, Superconductors
	Optically Short-Circuiting the switch	High Temperature Superconductor (High-Tc) bridge
	Nonlinear Transmission line (NLTL)	Electronic Circuits Consists NLTL
CW THz Radiation	Photomixing	PC Switch
	Difference Frequency Generation	Nonlinear Crystal
	Rotational Transitions	Far-Infrared Gas Lasers
	Streaming Motion & Population Inversion	P-Type Germanium Lasers
	Frequency Multiplication of Microwaves	Schottky Barrier Diodes
	Transitions in Superlattice	Quantum Cascade Lasers (QCL)
	Electron Interactive with a Travelling Electromagnetic Wave	Backward Wave Oscillator (BWO)
	Relativistic Electron Interaction with Transverse Magnetic Field	Free Electron Lasers (FEL)

2.3.1 Photoconductive Antenna Method for Generation

Photoconductive Antenna Method uses a PC antenna to generate THz radiation. In principle antenna structure consists of a semiconductor substrate, metal electrodes, and a hemisphere on it as seen in Figure 2.1. Metal electrodes with the gap in between, forms an antenna structure.

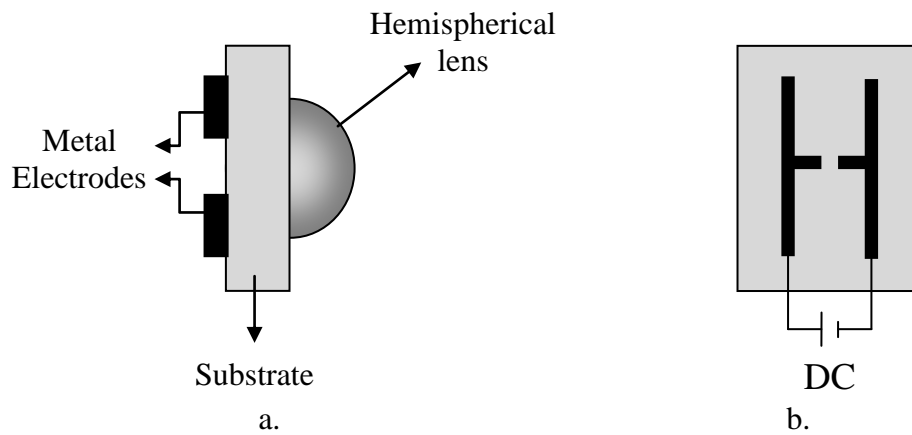


Figure 2.1 a) Side view of PC antenna b) Top view of PC antenna

A bias voltage is applied on the metal electrodes. Distance between the electrodes forms a gap and femtosecond optical pulse focuses to that gap. Meanwhile electron-hole pair is formed in the semiconductor. Once the optical pulse hits the antenna structure, electron-hole pairs form in the conduction band of the substrate. Then free carriers, which are accelerated by applied bias voltage, result as a photo current in the dipole.

This current is a function of time and the derivative of this current gives the resultant EM radiation in THz frequency. Electric field generation from a Hertzian dipole antenna is expressed as;

$$E(r, t) = \frac{l_e}{4\pi\epsilon_0 c^2 r} \frac{\partial J(t)}{\partial t} \sin\theta \propto \frac{\partial J(t)}{\partial t} \quad (2.1)$$

Where $J(t)$ is the current in the dipole, l_e the effective length of the dipole, ϵ_0 the dielectric constant of vacuum, c the velocity of light in vacuum, θ the angle from the direction of the dipole and r the distance from the dipole (r is greater than the emitted wavelength-far field) [4].

In order to have THz radiation, this process should happen in a subpicosecond time interval. Since optical pulse acts as a switch in the PC antenna, the laser pulse duration is related with switch-on time where the carrier life time of the substrate is related with the switch-off time. Other important parameters for a good PC antenna are high carrier mobility and high breakdown voltage. As well as the substrate properties, antenna structure also affects the PC antenna quality. Stripline, dipole, offset dipole, and bowtie are some examples for antenna structures.

Low temperature grown gallium arsenide (LT-GaAs), radiation damaged silicon-on-sapphire (RD-SOS), chromium-doped gallium arsenide (Cr-GaAs), indium phosphide (InP) are typical substrates for PC antenna. Among these substrates LT-GaAs has the shortest carrier lifetime with 0.3 ps. LT-GaAs and RD-SOS are the most commonly used substrates for PC antenna [1].

2.3.2 Optical Rectification for Generation

Optical rectification is a second order nonlinear optical process. In principle optical rectification is a reversed process of electro-optic (EO) sampling [34]. In order to use this process and to generate radiation, an applied electric field and EO crystals are needed. Applied electric field and generated radiation should be transient in the

generation medium. Semiconductors, organic and inorganic crystals are used as generation medium. Optical rectification process only occurs in the non-centrosymmetric crystals.

Femtosecond lasers are used as an applied field. Since femtosecond lasers consist of many frequencies, when the laser focused on the crystal difference-frequency generation occurs. The resultant polarization is proportional to the applied electric field by the factor of susceptibility. If the polarization is expanded in power series, optical rectification will be related with the second order term.

$$P(r, t) = \chi^{(1)}(r, t)E(r, t) + \chi^{(2)}(r, t)E^2(r, t) + \chi^{(3)}E^3(r, t) + \dots \quad (2.2)$$

where $\chi^{(n)}$ is the n^{th} order susceptibility tensor $E(r, t)$ is the incident electric field [3]. The radiated field is proportional to the second time derivative of the polarization. Hence, generation medium plays an important role in order to have broadband THz radiation. Other important properties that influence the THz radiation are phase matching, crystal thickness, absorption and dispersion. The orientation of the crystal is also important for THz radiation.

The maximum intensity is observed when the phase matching condition is satisfied. This is true when the group velocity of the optical beam is equal to the phase velocity of the THz beam. In addition to that, if the optical wave and THz wave propagates collinearly in the crystal, then this condition is called collinear phase matching.

Refractive index of the generation medium, which is crystal in this case, generally differs for optical frequencies and THz frequencies. This causes a velocity mismatch in the medium between these pulses at those frequencies. After the generation of THz in the crystal, if the perfect velocity matching achieved, then THz pulse should be amplified during the propagation in the crystal. However, it is difficult to achieve such a velocity matching. When the optical pulse is faster than the THz pulse, optical pulse leads THz pulse after a distance, which is called walk-off length (l_ω) [1].

$$l_\omega = \frac{c\tau_p}{(n_T - n_O)} \quad (2.3)$$

where τ_p is optical pulse duration, n_{gr} is optical group refractive index, n_T is THz refractive index and n_O is the optical refractive index of the crystal.

As an example the following formulas reflect how the index of refraction changes with optical and THz frequency for the crystal $\langle 110 \rangle$ ZnTe which is extensively used in THz generation and detection and has also been used in this thesis.

$$n_O^2(\lambda) = 4.27 + \frac{3.01\lambda^2}{\lambda^2 - 0.142} \quad (2.4)$$

$$n_T^2(v_{THz}) = \frac{289.27 - 6v_{THz}^2}{29.16 - v_{THz}^2} \quad (2.5)$$

Walk-off length should be longer for a crystal; however the thickness of the crystal should be shorter than walk-off length for a generation crystal [1]. If the crystal thickness is smaller, then the radiation strength will be smaller [28].

Nonlinear properties of the medium, absorption of both optical and THz radiation in the medium and phase matching condition should be considered for the decision of the crystal. $\langle 110 \rangle$ ZnTe, $\langle 110 \rangle$ CdTe, $\langle 110 \rangle$ GaP, $\langle 111 \rangle$ InP and $\langle 100 \rangle$ oriented GaAs are commonly used as semiconductors. They are phase matched at the following wavelengths respectively; 800nm, 970nm, 1000nm, 1220nm 1350nm. LiNbO₃ is the most common inorganic crystal and 4-N-methylstilbazolium tosylate (DAST) is the most common organic crystal [1, 28, 35].

2.4 Detection of THz Radiation

Since THz radiation occurs in two different ways, detection is also divided into two parts; coherent and incoherent detection. In coherent detection amplitude and phase of the radiation are detected, whereas in incoherent detection only intensity can be measured. Detection of phase and amplitude has great importance in spectroscopy. As a result, coherent detection is the most commonly used detection type. Widely used coherent detection types are free space electro-optic (EO) sampling,

photoconductive switching, photomixing, and heterodyne detection. First two methods are used for pulsed THz radiation and the last two is used for CW THz radiation. Most of the incoherent radiation is blackbody radiation, thus the incoherent detectors use thermal sensing techniques in principle. Bolometers, Golay cells, and pyroelectric devices are some examples or incoherent THz detectors [1].

2.4.1 Photoconductive Antenna Method for Detection

The detection of THz by using photoconductive antenna is based on the same principle with the generation; however one is the reversed process of the other. In the detection process there is no applied bias on the antenna. Optical pulse creates electron-hole pair on the substrate and this time free carriers are accelerated by the THz pulse. The rapid change of the conductivity by the movement of the free carriers creates a current. By measuring the current between electrodes of the antenna, THz pulse can be probed.

Generated THz radiation is proportional to carrier lifetime photoconductive antenna. This relation is expressed as follows,

$$Detection\ bandwidth \sim \frac{1}{\Delta\tau} \quad (2.6)$$

$\Delta\tau$ is carrier life time of the PC antenna. For example in our antenna generation system discussed in chapter 3, if we had used the antenna for THz detection our bandwidth would be limited by the antenna properties as such: the carrier lifetime is 400fs so that the maximum detectable THz bandwidth is 2.5THz.

In order to use a PC antenna in the detection process, the carrier lifetime of the substrate should be shorter as compared to the rate of change of the THz pulse.

2.4.2 Electro-Optic (EO) Sampling

Electro-optical detection is based on phase modulation measurement. Optical and THz pulse both propagate in the EO crystal. A phase modulation is induced on the optical pulse by the THz pulse electric field. The phase modulation on the optical pulse is measured by analyzing the polarization of the beam, otherwise known as an ellipsometry technique [36]. Terahertz pulse creates a birefringence in the detector crystal. This change causes a change in polarization of the optical pulse [37].

THz pulse and the optical pulse propagate collinearly in the crystal. The birefringence due to the THz pulse on the detector crystal is sensed by the optical pulse. As a result of that the optical pulse changes its polarization (typically to elliptical state) where after the minor and major components of the polarization are detected by photodiodes.

This technique is limited by the time duration of the optical pulse, second order susceptibility of the detector medium, transparency of the crystal at THz and optical frequencies and phase matching condition [38, 39].

In the next chapter we discuss the development of a time domain THz spectrometer based on antenna generation and electro-optic detection.

CHAPTER 3

THz TIME DOMAIN SPECTROMETER WITH PHOTOCONDUCTIVE ANTENNA GENERATION

THz Time-Domain Spectrometer is a type of THz Spectroscopy system, which uses the time domain aspects of the system. Optical properties such as absorption coefficient, refractive index, and conductivity of various materials can be easily acquired by this technique. The amplitude and phase are calculated by measuring the electric field. This in return provides the absorption coefficient and the refractive index of the material analyzed. Also the optical properties in addition to fingerprint spectra of materials can be obtained at THz frequencies.

In this chapter, first, the THz time domain spectrometer we built is described. This particular spectrometer uses Photoconductive (PC) antenna for generation and electro optic (EO) crystal for detection. Following the calculation methods for absorption coefficient and refractive index, a system modification towards characterizing small samples is discussed. Finally, absorption coefficient and refractive index of various materials are calculated and the results are presented.

3.1 SYSTEM OVERVIEW

In this study THz Time Domain Spectrometer was constructed with photoconductive antenna method for THz generation and Electro optic (EO) method for THz detection. From here on this system is referred as “Antenna-crystal System”.

Setting up a THz Time Domain System could be expensive however it is a very useful analytical tool, so that the benefit overcomes the cost. Ti:Sapphire mode-lock laser was used as an optical source for the system. In order to maintain laser stability and quality, the system is constructed in a clean room at 19 °C. The temperature is kept under control by an air-conditioner system.

The system consists of several optical components such as; mirrors, lenses, filters, wave plate, and Wollaston prism. Like optical components, electrical components are also necessary for the spectrometer. Function generator, balanced photodiode, lock-in amplifier, and computer are the electronic components of the system.

3.1.1 Detailed Description of the Spectrometer

The system used for this thesis is shown in Figure 2.1. From the beam splitter laser pulse is divided into two arms (paths): generation/pump arm and detection/probe arm. Both of these arms start at the beam splitter and end at the crystal. Former arm follows the path from the component *b* to component *i* (*b*, *M*₂, *M*₃, *M*₄, *M*₅, *c*, *d*, *e*, *f*, *PM*₁, *PM*₂). Latter arm follows the path through *b*, *g*, *h*, *M*₆, *i* and *j*.

Components through *M*₇ to *n* (*M*₇, *j*, *k*, *l*, *n*) were used for data collection. The component *n* (computer) was used to record data for further analysis.

The components of the instrument shown in Figure 3.1 are listed below:

- a) Ti: Sapphire Mode-Lock Laser (Coherent Verdi-V5 pumped Femtosource Femtolaser Scientific XL-Pro)

b) Beam splitter

Generation arm

M₂- M₅: Mirrors

c) Attenuation filter (0,6)

d) Leitz 16x objective (PLAN)

e) Batop PCA 44-06-10-001 photoconductive antenna (PCA)

f) Agilent Technologies LXI-33220A Function generator

PM₁ – PM₂: Off axis parabolic mirror (OAPM)

Detection arm

g) Attenuation filter (0.3)

h) Corner Cube and translation stage with motor controller Thorlabs BSC 103

M₆: Mirror

i) Lens with focal length 200 mm

j) <110> cut ZnTe crystal

Data Acquisition components

M₇: Mirror

k) $\lambda/4$ Quarter wave plate

l) Wollaston Prism

m) New Focus 2307 Large-area Balanced Photoreceiver

n) Stanford Research System SR830 Lock-in Amplifier

o) Computer with software

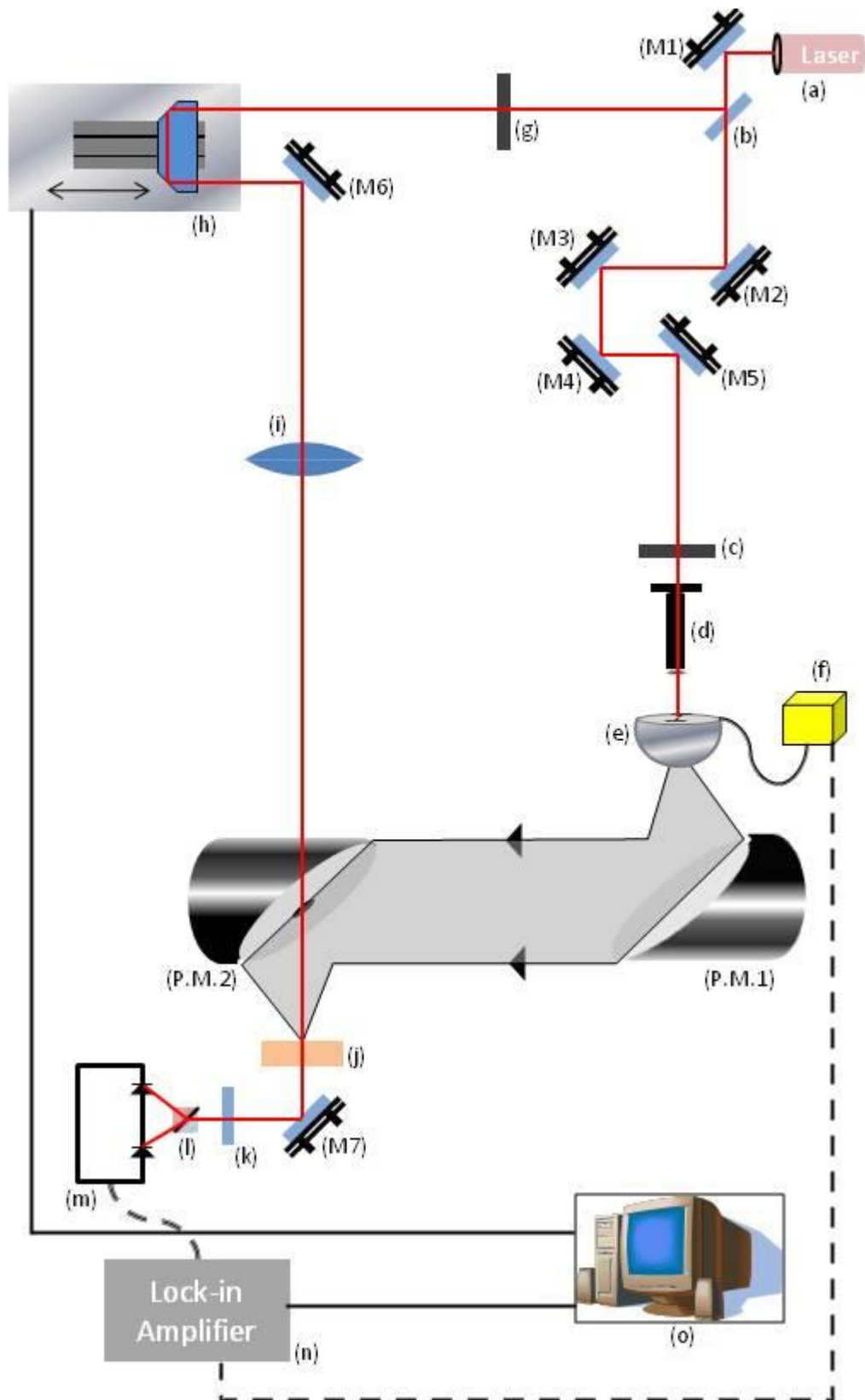


Figure 3.1 Schematic representation of the system

The ultra fast laser was used to generate and detect the THz radiation. The Ti: Sapphire mode-locked laser specifications for this experimental setup are: ~135mW power with 800 nm wavelength at center frequency. Time duration is 30 fs with 75 MHz repetition rate.

25:75 beam splitter (component *b* in figure 3.1) was used to divide the laser beam into two arms. In order to detect the THz radiation, the visible and the THz beam should reach the detector at the same time. To facilitate the detection four mirrors (M2, M3, M4 and M5 in figure 3.1) were placed in the generation arm to equate the path length with detection arm. In the generation arm, after these mirrors, an absorptive natural density filter (OD: 0.6) (component *c* in figure 3.1) was used to reduce power coming towards the PC antenna (component *e* in figure 3.1). By doing so, the PC antenna is protected. This natural density filter transmits the incoming laser by 25% [40]. The transmitted laser was focused on the PC antenna with a 16x objective.

The photoconductive antenna (PCA) used for this system is a dipole antenna with butterfly type. It is manufactured by Batop and the antenna is mounted on a LT-GaAs substrate. Dimensions of the electrodes are shown in the Figure. 3.2 Length of the antenna is 44 μm , width of the antenna is 10 μm and the gap between the electrodes is 6 μm (see Figure 3.2) [41]. Incident laser pulse should be focused to the antenna gap.

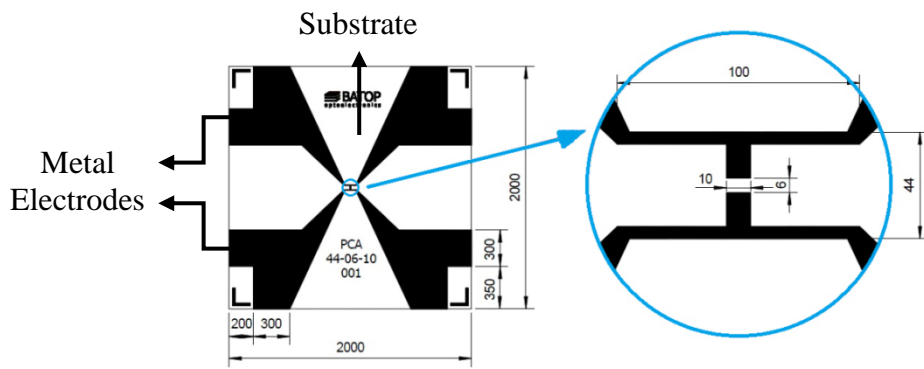


Figure 3.2 Dimensions of the PCA 44-06-10-001 (units are in micrometers) [17]

The electrodes along with the substrate form a square chip (see Figure 3.3a). This chip is glued on hyper-hemispherical silicon lens. Lens is made of high resistivity float zone silicon (HRFZ-Si), which is the most commonly used material in the THz range. High, frequency independent transmission is an additional advantage of this lens material. Silicon lens helps to reduce the divergence of the radiated pulse. Structure of the antenna can be seen in Figure 3.3

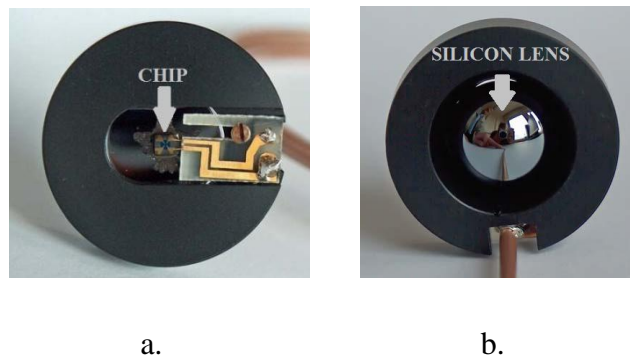


Figure 3.3 Photographs of PC antenna

a. Front view (laser side) b. Back view (THz side) [17]

While the laser (optical) pulse is focused on the chip on the front side, THz pulse is emitted from the back side. Laser pulse should be focused on the gap between electrodes. Since the gap is $6 \mu\text{m}$, it is important to align the laser each time it is turned on. In order to compensate laser fluctuations PCA is placed on a xyz translation stage. This stage is also useful for the alignment of the laser.

In order to have optimum performance from the PCA, not only the focus on the dipole gap should be precise, but also the power of the incoming laser pulse has to be sufficient so as to bridge the gap. The electrical and optical excitation parameters of the PC antenna are shown in Table 3.1.

Table 3.1 Electrical and Optical excitation parameters for PCA [41]

Electrical Parameters		Optical Excitation Parameters	
	Standard Ratings		Standard Ratings
Dark resistance	25 M Ω	Excitation laser wavelength	800 nm
Dark current @ 10 V	400 nA	Optical reflectance	5 % @ 800 nm
Voltage	20 V	Optical mean power	30 mW
		Optical mean power density	100 kW/cm ²
		Carrier recovery time	400 fs

PCA should be supplied with a voltage supply. For the experiments presented in this document a function generator (component *f* in Figure 3.1) was used. It supplied peak to peak 10V square wave with 2.5 kHz frequency to the antenna. It was also connected to the lock-in amplifier to provide frequency information as reference.

After the THz generation, the radiation was collimated by off-axis parabolic reflectors (P.M.1 and P.M.2 in figure 3.1). Collimated beam was also collected by an off-axis parabolic reflector and focused onto the ZnTe crystal (component *j* in figure 3.1), where the generation arm ends. These two reflectors have focal length of 119.4 mm. Reflectors are made out of electro-formed nickel [42].

In the detection arm, the reflected beam from the beam splitter is directed to the corner cube. Corner cube is placed on a motor controlled translation stage (component *h* in figure 3.1). This stage is controlled by a computer with a pre-designed interface. This stage provides path difference during the measurements which is used as delay line. Next, optical beam is focused onto detection crystal (component *j* figure in 3.1) by a lens (component *i* in figure 3.1) with a focal length

of 200mm. The beam passes through one of the reflectors. In order to have more symmetric and better aligned setup, a hole was drilled in the middle of the reflector (component P.M.2 in figure 3.1).

After the detection crystal, a mirror (M7 in figure 3.1) is used to direct the beam to quarter wave plate (component k in figure 3.1), then to Wollaston prism (component l in figure 3.1) and balanced photo detector (component m in figure 3.1). Quarter wave plate was used to detect the changes in polarization. The incoming polarization was separated into its components by Wollaston prism. After the Wollaston prism, two beams illuminated the balanced photo diodes. Photodiode was connected at the lock-in amplifier.

Lock-in amplifier (component n in figure 3.1) is used in the case of weak signals. A lock-in amplifier can detect signals in the order of nanovolts (nV) or nanoampers (nA). Both voltage and current measurements are possible with lock-in amplifier. Lock-in amplifier gathers data according to the reference frequency. Frequencies other than the reference frequency do not affect the measurement [43]. Thus, it locks the reference frequency to the desired frequency. Lock-in amplifier also uses phase information.

All the information gathered from lock-in amplifier with the translation stage is controlled by the computer (component o in figure 3.1). With the help of a computer program, the THz waveform is obtained.

3.1.2 Data Collection

Optical beam follows two paths in the system. After the beam splitter, laser beam is focused onto the photoconductive antenna. The incoming power of the laser beam is reduced to the optimum operation conditions for the PC antenna. Thus, before the PC antenna an O.D. 0.6 attenuation filter is used to protect the antenna structure. Off-axis parabolic reflector is used to collimate the generated THz pulse. Then, the collimated beam is focused on the detection crystal, again with an off-axis parabolic

reflector. The path that is followed from beam splitter through PC antenna to detection crystal is called the pump/generation arm.

The other laser beam that is reflected from beam splitter is also focused on the detection crystal, following the path through the corner cube. This path is called the probe/detection arm. On the detection arm a delay line is placed with a motor controlled translation stage. This delay line provides time and path difference between optical and THz beam to profile THz waveform. After the crystal, quarter wave plate changes the polarization of the optical beam and Wollaston prism separates polarization into its components. If optical beam and the THz beam are both incident on the crystal, then the polarization after the $\lambda/4$ waveplate will be elliptical. Thus the components of the polarization must be different. This difference is detected with the balanced photodiode.

The motor controlled translation stage is connected to the computer with lock-in amplifier. Balanced photodiode and function generator supply the required information to the lock-in amplifier, which are the reference frequency and the voltage. Eventually all of the data is collected by the computer and processed by LabView software.

The motor controller has a user interface and it is controlled by LabView program. This software helps to manage the step size, time duration, and the scan distance. Step size is the measure of the distance travelled by the translation stage. This path difference also results in the time difference of the optical pulse. Time duration is the amount of time that the motor delays between two consequent moves. It helps to synchronize the motor and the lock-in amplifier to prevent data losses. Scan distance is the length of distance travelled by the translation stage. The step size and scan distance give the total time of the motion. The voltage value gathered from photodiode can be plotted with respect to total time, which gives the THz waveform. The data recorded in the computer can be used for further calculations. Calculations from this data will be explained in the next section.

The software parameters used for this antenna/crystal system is, 15 μm step size, 15260 μm total scan distance and 600 ms time duration. According to total scan

distance 1024 data points are collected. It is important to have data to the n^{th} power of 2 for Fourier Transform. The THz waveform of this system both in time domain and frequency domain is seen in Figure 3.4 and Figure 3.5, respectively.

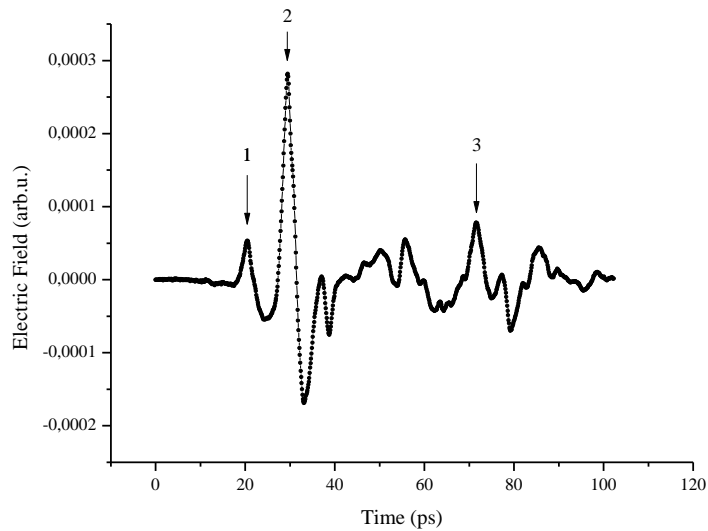


Figure 3.4 Temporal waveform of THz radiation measured with THz-TDS

In the temporal waveform the three pulses are seen in Figure 3.4. The biggest pulse which is shown in figure with arrow number 2 is the main THz pulse. Before the main pulse a reflection of optical pulse is seen (arrow number 1). The reason of this reflection is the back reflection from the detection crystal. The third pulse is the reflection of the THz pulse coming from detection crystal.

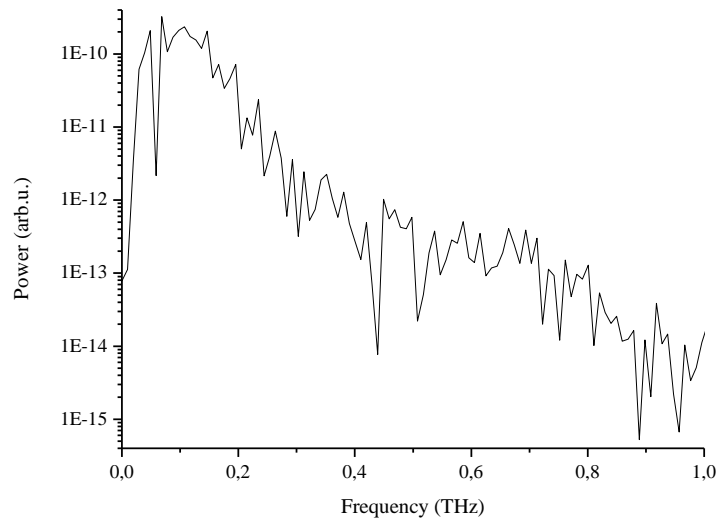


Figure 3.5 Power spectrum of the temporal waveform shown in Figure 3.4

Power spectrum is seen in Figure 3.5. Power spectrum was obtained from the data seen in Figure 3.4. Bandwidth of the spectrum can be determined from power spectrum. System typically has ~ 1.5 THz frequency bandwidth however the figure above shows a bandwidth of ~ 0.9 THz.

3.2 THEORY AND ANALYSIS

Measured time domain data can be analyzed by applying Fourier Transform. Time domain data is basically the THz waveform, which is the detected electric field with respect to the delay time. The time dependence of the electric field can be converted into frequency dependence by Fourier Transform. Thus, the frequency dependent electric field can be expressed as [3];

$$E(\omega) \equiv A(\omega)e^{-i\phi(\omega)} = \int dt E(t)e^{-i\omega t} \quad (3.1)$$

where $A(\omega)$ is amplitude of the electric field in frequency domain, and $\phi(\omega)$ is the phase of the electric field in frequency domain. As it seems from the formula, Fourier Transform provides the amplitude and phase information that are characteristic to THz Time Domain Spectroscopy. By using these parameters absorption coefficient and the refractive index can be calculated.

Spectral range of the Fourier analysis is determined by the delay time. The amount of time it takes for the optical beam to travel 300 μm is 1 ps. Thus, change in the optical path can be referred as delay time. The time interval (Δt) between each measurement defines the sampling rate ($f_s=1/\Delta t$). Spectral range starts from $(-f_s/2)$ and ends at $(+f_s/2)$. The spectrum is symmetric at the center frequency ($f_s=0$). Bandwidth of the THz system can be obtained from this analysis.

The THz radiation traveling in the air or a holder without the sample gives the reference waveform in time domain. Similarly the THz radiation that passes through the sample gives the sample waveform. Reference and the sample waveforms should be gathered from the same starting point. This is important to have correct phase shift measurements. By applying Fourier Transform (FT) to the time domain data (both reference and sample waveform), spectral information is obtained, such as phase and amplitude. The comparison of the phase and amplitude within each reference FT and sample FT, provides optical properties of the materials studied. Phase difference in general results in the refractive index, where power ratio results in absorption coefficient.

In order to calculate these values, reference and sample, THz waveform is collected. When the sample is present in the spectrum, it takes more time to travel through the sample for THz pulse. As a result, when compared to the reference pulse, THz pulse that passes through the sample appears later. This causes the time difference in the waveform. This time difference results in the phase difference in the frequency domain.

The refractive index is composed of real and imaginary parts.

$$\tilde{n}(\omega) = n_r(\omega) + in_i(\omega) \quad (3.2)$$

$n_r(\omega)$ is real part and $n_i(\omega)$ is the imaginary part of refractive index where,

$$n_r = \frac{1}{kl} (\phi(\omega, l) - \phi(\omega)) \quad (3.3)$$

$$n_i = \frac{1}{kl} \left(\ln \left(\frac{E(\omega, l)}{E(\omega)} \right) \right) \quad (3.4)$$

k is wave vector, l is the sample thickness, $\phi(\omega)$ is phase of the reference. Here, real part gives the refractive index and imaginary part gives the absorption coefficient.

The real part discussion here is considered as vacuum. If the experiment is performed in air then, corrected real part of refractive index should be as follows,

$$n_r(\omega) = 1 + \frac{1}{kl} (\phi(\omega, l) - \phi(\omega)) \quad (3.5)$$

3.3 FOCUSING OF THz RADIATION ON SMALL SAMPLES

In most of the cases THz-TDS systems are used for laboratory applications. Depending on the sample size and experimental conditions the system may require modifications.

In the Time-Resolved Spectroscopy system, the THz pulse as well as a different light source is focused onto the target sample. Those systems are used for photoexcitation applications. In order to photoexcite a material, an incident beam should be focused to illuminate the sample as THz pulse. In addition to that, THz pulse beam size should be at least as small as the incident beam.

In our experiment two polymethylpentene (TPX) lenses were used to focus the THz pulse. The diameters of the lenses were 50 mm and focal lengths of the lenses were

100 mm. TPX was one type of material that can be used as lenses for THz systems. TPX was used due to its transparency at THz frequencies. Also, it can be shaped into lenses, windows, etc. Furthermore TPX is also a very light material with a density of 0.83 g/cm^3 [44].

These TPX lenses were placed between the off-axis parabolic reflectors in the system. In the Figure 3.6 TPX lenses are indicated with red arrow in the schematic representation of the THz-TDS system.

The beam parameters of the focused THz pulse can be calculated through the equations shown in Table 3.2 and the parameters in the equations are shown in the Figure 3.7.

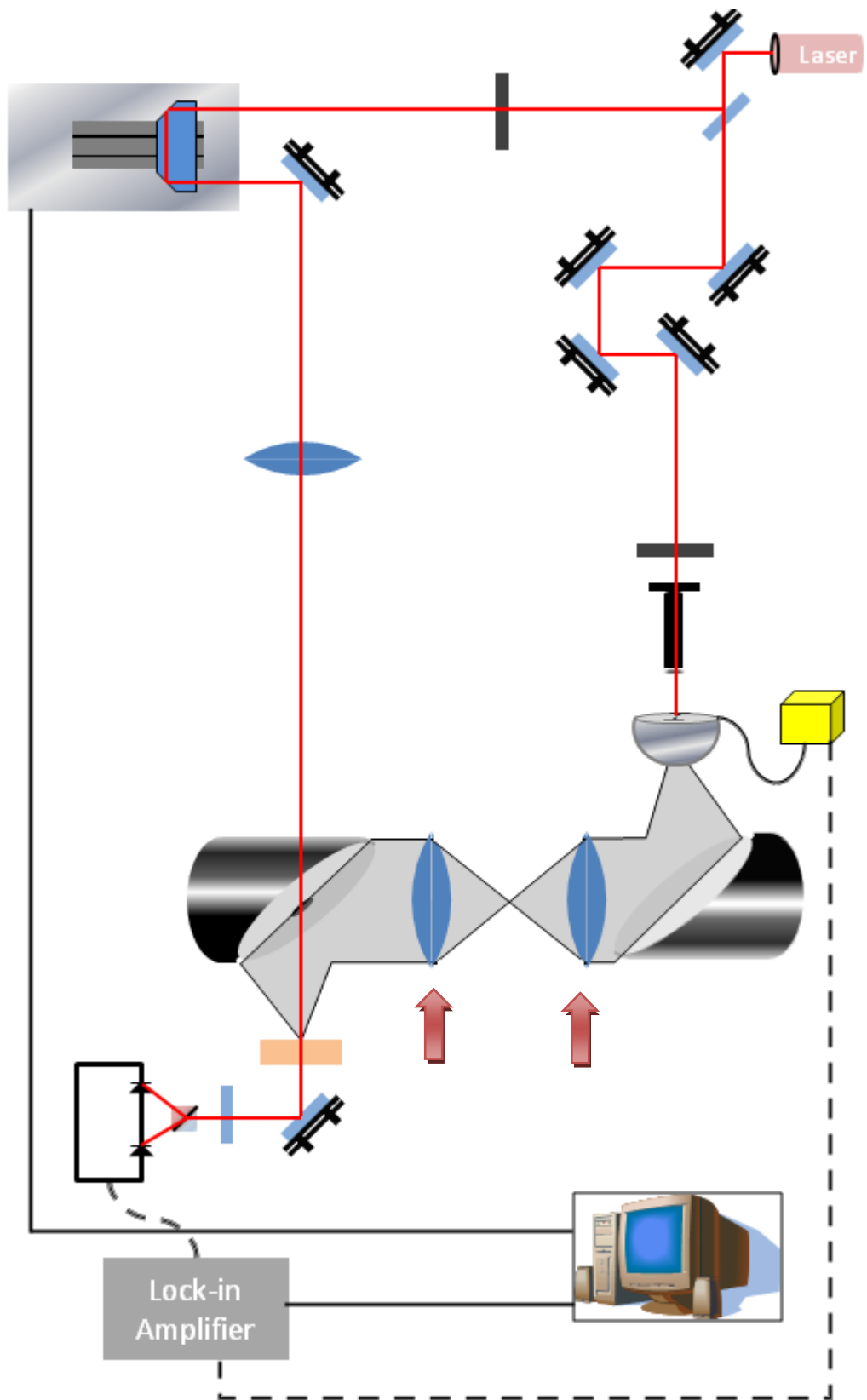


Figure 3.6 THz-TDS system with THz focusing lenses

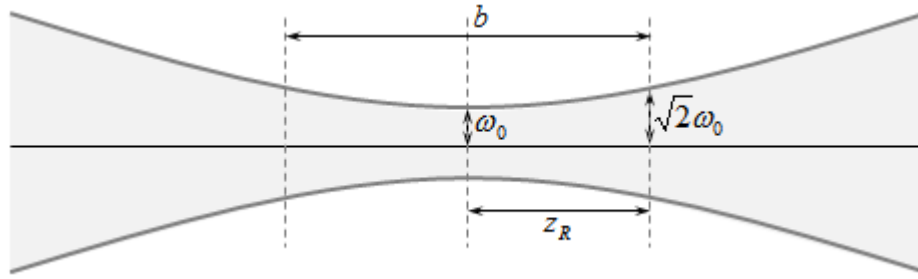


Figure 3.7 Spot size and confocal parameters

Table 3.2 Table of spot size and confocal parameter relations

Equations	Parameters	Eqn.
$\theta = \frac{1.22\lambda}{d_{in}}$	θ : angular divergence of the beam λ : incoming wavelength d_{in} : entrance beam diameter	(3.6)
$d_{out} = f\theta$	d_{out} : exit beam diameter f : focal length of the lens	(3.7)
$\omega_0 = \frac{d_{out}}{2}$	ω_0 : beam waist	(3.8)
$z_R = \frac{\pi\omega_0^2}{\lambda}$	z_R : Rayleigh range	(3.9)
$b = 2z_R$	b : confocal parameter	(3.10)

The known parameters for the TPX lenses are: entrance beam diameter (50 mm), focal length (100 mm), and wavelength (2000 μm for 0.15 THz). For our system the peak spectral power occurred at 0.15 THz:

$$\theta = \frac{1.22 \times 2000 \times 10^{-6}}{50 \times 10^{-3}} = 0.049 \text{ rad} \quad (3.11)$$

$$d_{out} = 100 \times 0.049 = 4.9 \text{ mm} \quad (3.12)$$

$$\omega_0 = \frac{4.9}{2} = 2.45 \text{ mm} \quad (3.13)$$

$$z_R = \frac{\pi(2.45)^2 \times 10^{-6}}{2000 \times 10^{-6}} = 0.009 \text{ m} \quad (3.14)$$

$$b = 2 \times 0.009 = 0.018 \text{ m} \quad (3.15)$$

In the system with these TPX lenses THz was focused on a spot of 4.9 mm in diameter. Rayleigh range and confocal parameter were calculated as 9.0 mm and 18.0 mm, respectively.

The transmittance of TPX lens at 1 THz frequency (or 300 μm wavelength) is around % 85 [44]. The refractive index of TPX lenses are 1.46 at the same frequency. Thus, when these lenses are placed in the system, the THz pulse amplitude will decrease. Similarly, if any component is placed in the THz pulse path, the pulse will arrive later which means that it will occur at a later in time in the waveform.

Lenses were placed between the two off-axis parabolic reflectors (see Figure 3.6). First TPX lens was used to focus THz pulse onto the target and second one was used to collimate the transmitted pulse. In order to define the position of the THz focus, an iris was used. According to calculated beam diameter iris opening was fixed. At the focus, with a proper iris height and opening THz pulse was passed without any loss at the peak value.

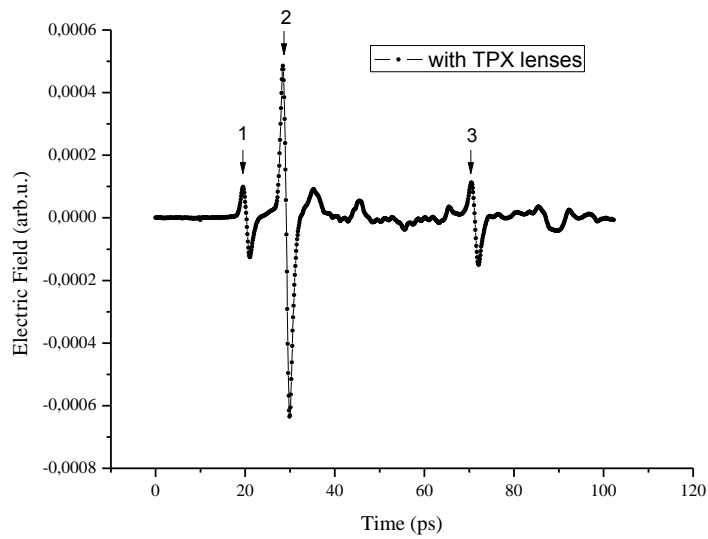


Figure 3.8 Temporal waveform of THz radiation collected by THz-TDS system with focusing lenses.

The temporal waveform of the THz system with focusing lenses is seen in Figure 3.8. Since the THz pulse is focused in this waveform THz pulse is shifted by 180 degrees (compare with Figure 3.4). In the waveform there are three pulses. The biggest pulse (denoted as 2) is the main THz pulse. Before the main pulse a reflection of optical pulse is seen in Figure 3.8 with arrow number 1. The reason of this reflection is the back reflection from the detection crystal of the probe beam. The other pulse which is denoted as 3 is the reflection of the THz pulse coming from the back reflection of the detection crystal. Addition to that, thickness of the detection crystal can be calculated from the time difference between the main THz pulse (pulse number 2) and the reflection of the THz pulse (pulse number 3).

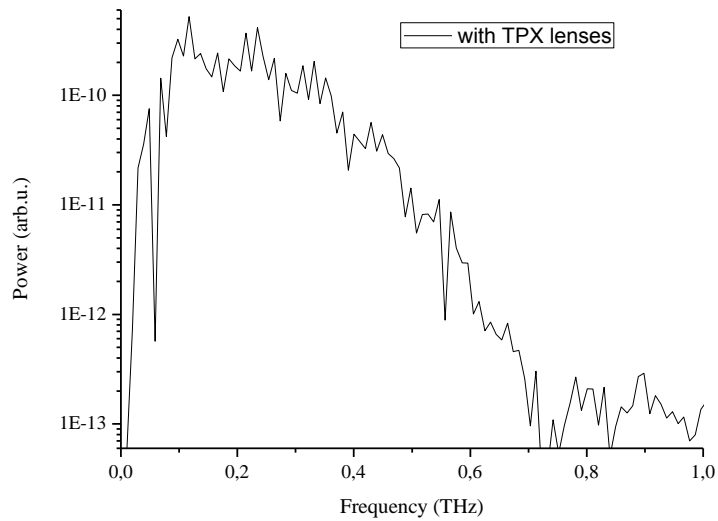


Figure 3.9 Power spectrum of the temporal waveform shown in Figure 3.8

Power spectrum shows that the bandwidth of the spectrum is ~ 0.8 THz as is seen from Figure 3.9.

3.4 EXAMPLE MEASUREMENTS

In the modified antenna-crystal THz-TDS system various mineral samples were investigated. Absorption coefficient and the refractive index of these samples were calculated. Calculations were done according to the discussions in section 3.2.

Sample analyses were grouped as chemical samples based on the source. The samples that were analyzed are mainly dietary supplements. There were two selenium samples with different thicknesses manufactured by a commercial company (A). The other selenium sample was from a different commercial company (B), named as white selenium. The fourth chemical sample was vitamin B₁₂ from a third

company (C). The types of the samples used in the system, name of the samples, and thickness of the samples are indicated in Table 3.3.

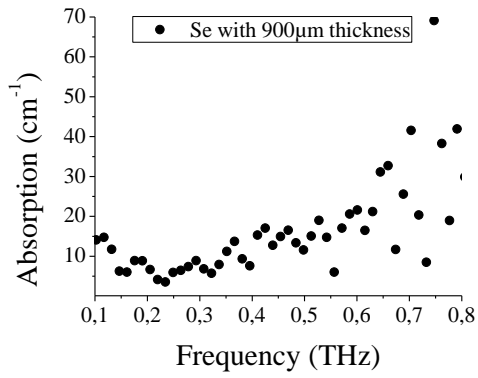
Table 3.3 Specifications of the samples

Type	Number	Sample name	Sample Thickness (μm)
Chemical Samples	1	Selenium1	900
	2	Selenium2	2530
	3	White selenium	700
	4	Vitamin B12	1250

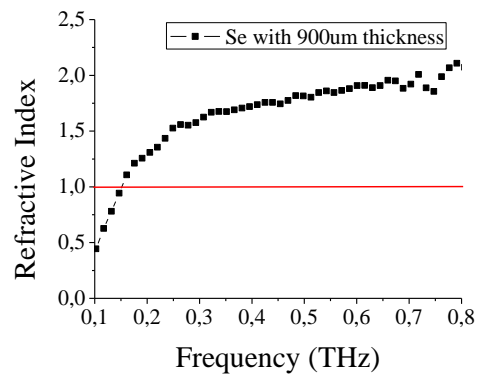
The first two samples were prepared from 200 mcg company A Selenium tablets by grinding them into power form and then pressing into pellets by applying a pressure of 10 MPa (The press machine was located at Central Laboratory facility at METU). Two pellets with different thicknesses were made. A similar procedure was applied to the third (company B) and fourth (company C) tablets however; the tablets were made at a single thickness.

Sample analysis starts with the time domain data. Both the reference and sample data were plotted to see the changes in phase and amplitude. After that, from a series of calculations absorption coefficient and refractive index of studied materials were calculated.

In all of the calculations usable data was collected up to 0.8 THz. Sample analysis of Selenium1, Selenium2, White selenium, and Vitamin B can be seen in the Figure 3.10a-b, Figure 3.11 a-b, Figure 3.12a-b, and Figure 3.13a-b, respectively.



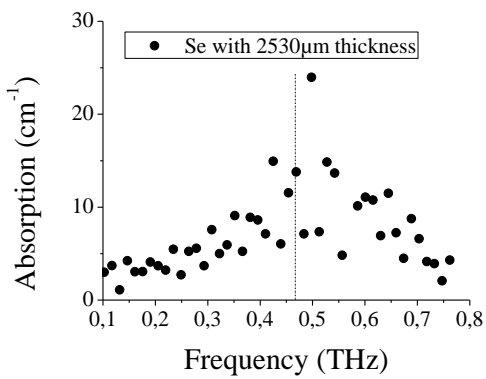
a.



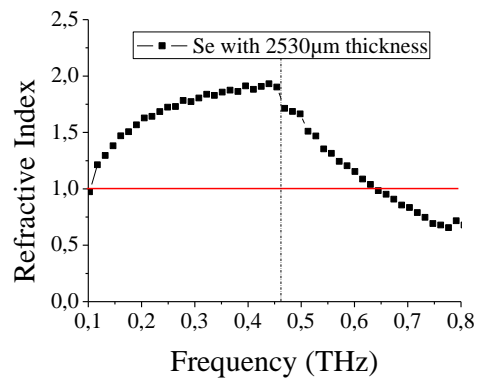
b.

Figure 3.10 Sample Analysis of Selenium1

a. Absorption Coefficient b. Refractive index



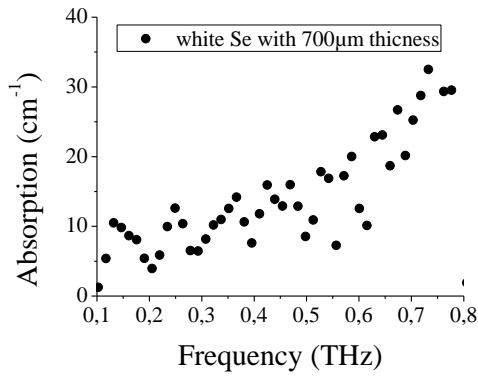
a.



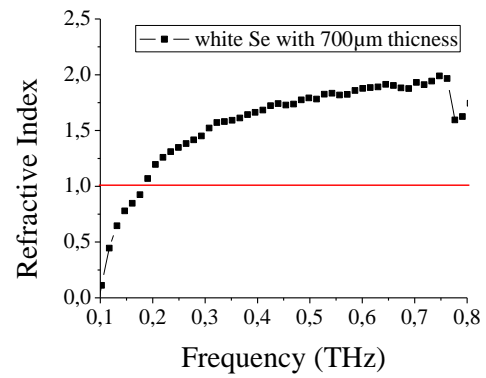
b.

Figure 3.11 Sample Analysis of Selenium2

a. Absorption Coefficient b. Refractive index



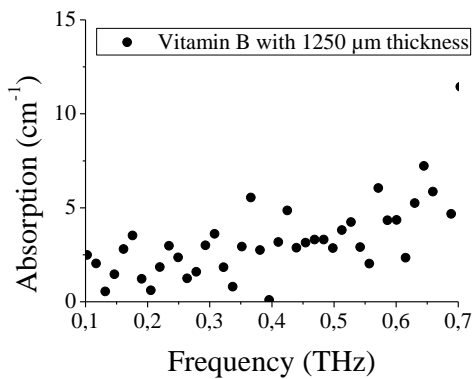
a.



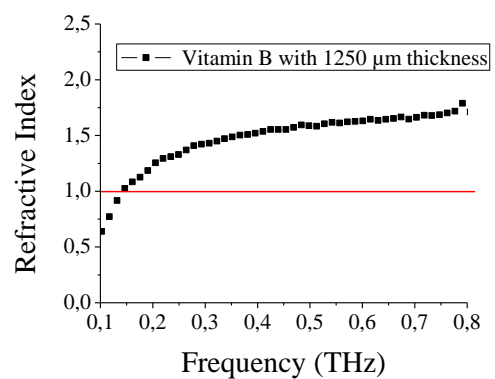
b.

Figure 3.12 Sample Analysis of White Selenium

a. Absorption Coefficient b. Refractive index



a.



b.

Figure 3.13 Sample Analysis of Vitamin B

a. Absorption Coefficient b. Refractive index

Previous figures show the calculations of the samples. In refractive index graphs a red line was placed as a reference line, since the experiments were performed in air.

Figure 3.10 and Figure 3.11 belongs to the same sample with different thicknesses. Calculation of refractive index of those samples gives the same result. However, with thicker sample a cut-off frequency appears. The cut-off frequencies are shown with a dashed line in Figure 3.11.a and Figure 3.11b. The other Selenium sample prepared from different supplement gives comparably same refractive index with first two Selenium samples.

3.5 DISCUSSION

In this system photoconductive antenna was used for THz generation and electro-optic sampling was used for THz detection. The bandwidth of the antenna-crystal system was approximately 1 THz. Bandwidth of the system was optimized with off-axis parabolic mirrors. Two TPX lenses were used to focus THz beam in order to analyze different samples. Dietary supplements were used as target samples in the system. Absorption coefficient and refractive index of these samples were analyzed. The sample thickness was found to be important in order not to lose higher frequencies.

Bandwidth of the Antenna-crystal system was limited with the optical excitation parameters of the emitter antenna as well as the system optical configuration. Most samples show features at frequencies above 0.5 THz. Our bandwidth does not cover the absorption spectra of most samples that we would like to investigate. For this reason a new system had to be constructed. This new setup is discussed in the next chapter. However, for antenna-crystal system, as will be seen in the next chapter the signal to noise ratio is much higher than crystal generation methods due to the higher THz power generated, which is an advantage of this system.

The detection method of the antenna-crystal system which was not discussed here is the same as the crystal generation system and is covered in Chapter 4.

CHAPTER 4

THz TIME DOMAIN SPECTROMETER WITH CRYSTAL GENERATION

In this chapter, a THz system where THz radiation is generated via optical rectification is described. An isotropic crystal (<110> ZnTe) is used for both generation and detection of THz radiation. Following the discussions of crystal choice, the principles of THz generation method is explained. Derivations of THz intensity and electric field are also demonstrated in this chapter. The chapter ends with discussions on the detection method.

4.1 SYSTEM INFORMATION

Optical rectification was used as generation method and electro-optic (EO) sampling method was used as detection method for constructing the THz Time Domain Spectroscopy (THz-TDS) system. In Figure 4.1 a schematic representation of this system is illustrated. The red line in the figure represents the path of the laser pulse and the arrows are indicating the direction of propagation of the laser pulse. Laser beam was split into two arms after the beam splitter. One of the arms forms the generation arm, and the other arm forms the detection arm, which is similar to the one described in the Chapter 3. Except for the components labeled as *c*, *d*, *e*, and *f* all others are the same components as had been described with the previous system.

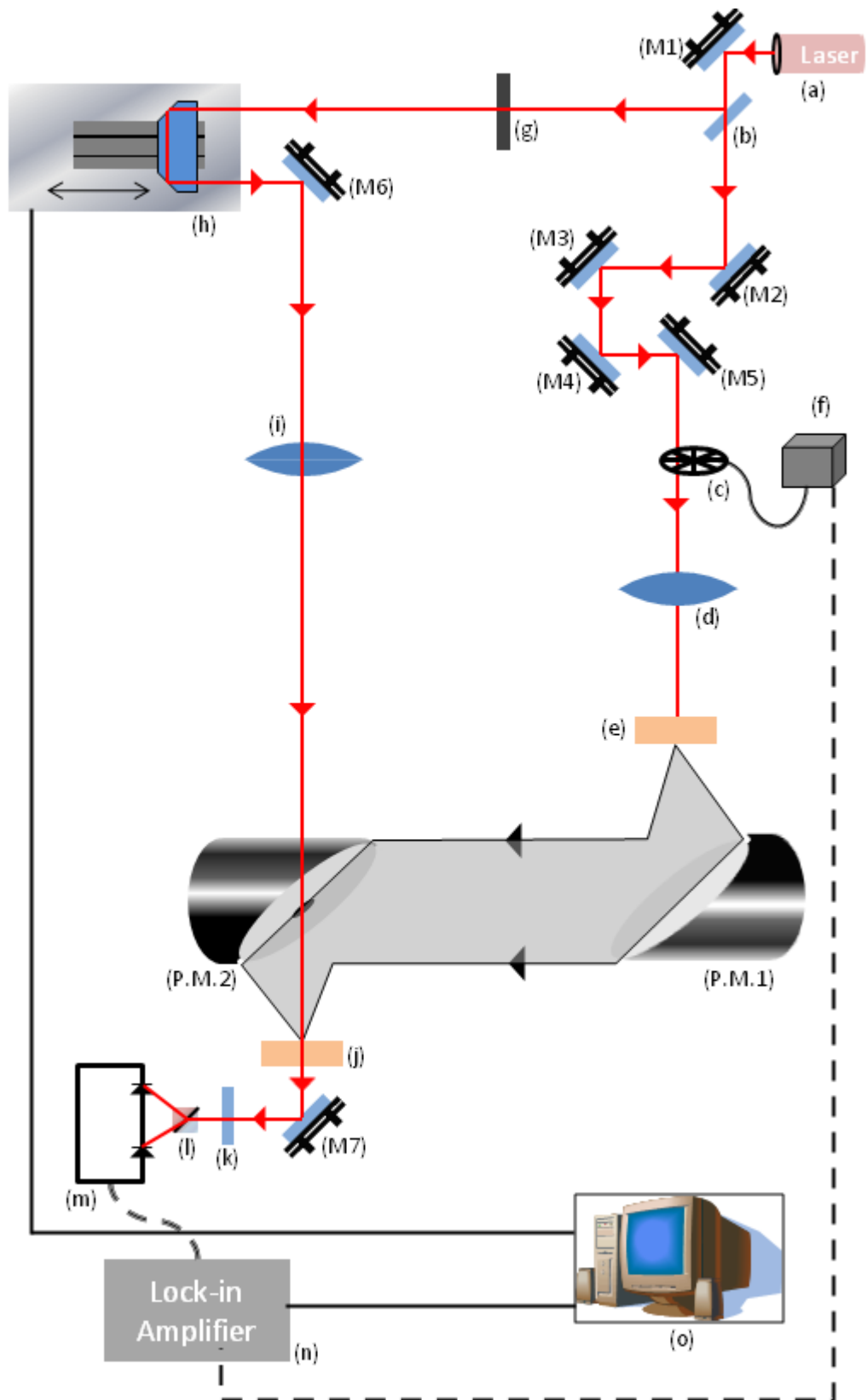


Figure 4.1 Schematic representation of the THz-TDS system with crystal generation

Ti:Sapphire mode locked laser produced ~135mW power, 800 nm wavelength at center frequency with 30 fs pulse duration. Laser beam was divided into two by a beam splitter. One of the laser beams passed through chopper (component *c*) with 2.5 kHz frequency and was focused on the generation crystal (component *e*) with a lens (component *d*) having focal length of 100 mm. Component *f* is used as an interface for the chopper. Other laser beam passed through time varying delay line and was focused on the detection crystal. Off- axis parabolic mirrors was used to collimate generated THz pulse and to focus the THz pulse onto the detection crystal. Optical pulse measurement was converted into electrical signals by a balanced photo diode which was connected to a lock-in amplifier. Lock-in amplifier was used to obtain phase sensitive measurements.

4.2 CRYSTAL GENERATION

Crystal generation is referred to as optical rectification. Optical rectification is based on a non-linear optical process. Crystal that is used in the THz systems serves as a non-linear medium. When an optical pulse interacts with this medium, a dc or low frequency polarization occurs [28, 45]. In the frequency domain, this polarization oscillates at the difference frequency generated by the optical pulse. Optical rectification occurs when the following conditions are satisfied. First, the crystal that is used for the non-linear medium should be non-centrosymmetric and also transparent at optical and THz frequencies. Second, the phase-matching condition, which is the condition when the group velocity of the optical beam is equal to the phase velocity of the THz beam, should be satisfied.

The advantage of the optical rectification is mentioned in the article written by Schmuttenmaer as “One advantage of optical rectification is that it is a nonresonant method and the THz pulse width is limited only by the optical laser pulse width (and the phonon-mode absorptions of the crystal), and not the response time of the material.” [45]

Considering these conditions mentioned above, crystal choice, calculations of radiated THz intensity, and radiated THz electric field is explained in the following sections.

4.2.1 Why ZnTe Crystal?

ZnTe crystal has the advantage of generating a much broader band THz spectrum compared to PC Antenna methods. Addition to that Ti:Sapphire laser with 800nm central wavelength was used in our system, which fulfills the phase matching condition for ZnTe crystal between 800nm wavelength and THz frequencies.

Refractive index of the generation medium, which is crystal in this case, generally varies for optical frequencies and THz frequencies. This causes a velocity mismatch in the medium between these pulses at those frequencies. After the generation of THz in the crystal, if the perfect velocity matching achieved, THz pulse should be amplified during the propagation in the crystal. However, it is difficult to achieve such a velocity matching. When the optical pulse is faster than the THz pulse, optical pulse leads THz pulse after a distance, which is called walk-off length (l_{ω}) [46].

$$l_{\omega} = \frac{c\tau_p}{(n_T - n_O)} \quad (4.1)$$

where τ_p is optical pulse duration, n_T is THz refractive index and n_O is the optical refractive index of the ZnTe crystal [34]. Optical and terahertz refractive index for ZnTe crystal can be obtained from equations 2.4 and 2.5, respectively.

The change of optical refractive index with respect to wavelength is seen in Figure 4.2, which is obtained from Eqn. 2.4. Similarly THz refractive index and walk-off length are calculated from Eqn. 2.5 and Eqn. 2.6, respectively. (See Figure 4.3 and Figure 4.4, respectively)

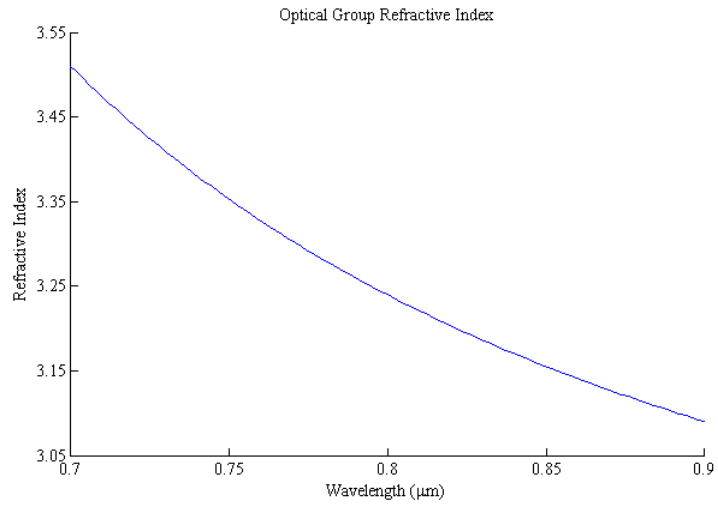


Figure 4.2 Optical Group Refractive Index

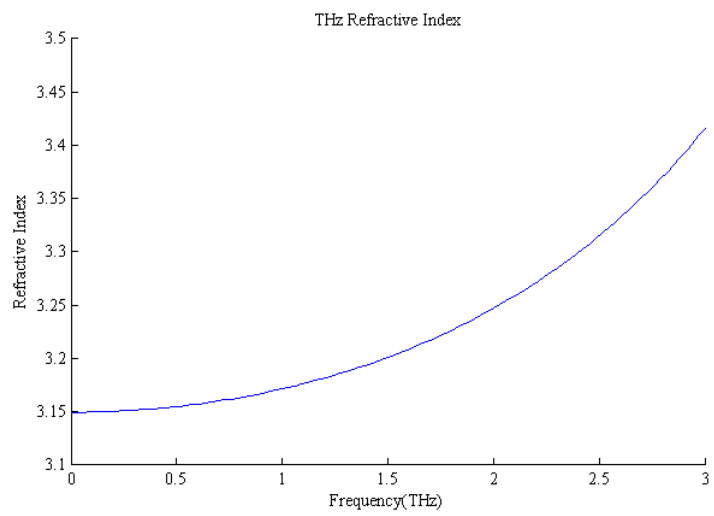


Figure 4.3 THz Refractive Index

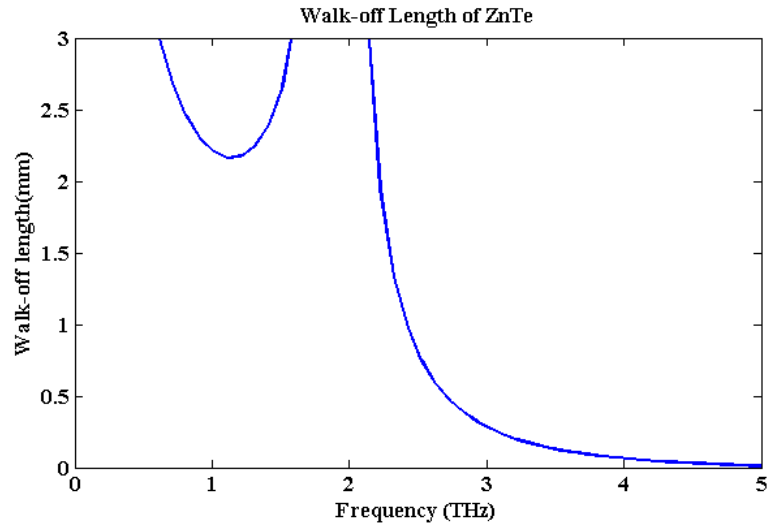


Figure 4.4 Walk-off length of ZnTe crystal

Walk-off length should be longer for a crystal; however the thickness of the crystal should be shorter than walk-off length for a generation crystal. If the crystal thickness is smaller, then the radiation strength will be smaller [28].

4.2.2 Generation with ZnTe Crystal

Optical rectification is a second order nonlinear optical process. In order to use this process and to generate radiation, an applied electric field and transparent crystals are needed. Applied electric field and generated radiation should be transient in the generation medium. Semiconductors, organic, and inorganic crystals are used as generation medium. Optical rectification process only occurs in the non-centrosymmetric crystals.

Femtosecond lasers are used as source of an applied field. Since femtosecond lasers consist of many frequencies, when the laser focused on the crystal difference-

frequency generation occurs. The resultant polarization is proportional to the applied electric field by the factor of second-order susceptibility (χ^2),

$$P_i^{(2)}(0) = \sum_{j,k} \epsilon_0 \chi_{ijk}^{(2)}(0, \omega, -\omega) E_j(\omega) E_k^*(\omega) \quad (4.4)$$

where $\chi_{ijk}^{(2)}$ is the n^{th} order susceptibility tensor for the nonlinear medium and the i, j, k are the indices [2]. The indices can be contracted in the form,

$$d_{il} = \frac{1}{2} \chi_{ijk}^{(2)} \quad (4.5)$$

$$\begin{array}{l} l = \quad 1 \quad 2 \quad 3 \quad 4 \quad 5 \quad 6 \\ jl = \quad 11 \quad 22 \quad 33 \quad 23,32 \quad 31,13 \quad 12,21 \end{array} \quad (4.6)$$

Starting with calculation of nonlinear polarization, intensity of the radiated THz pulse and electric field of the same pulse can be calculated. Thus, first the nonlinear polarization is calculated for $i = 1$,

$$\begin{aligned} P_1 = \epsilon_0 [& \chi_{111}^{(2)} E_1 E_1 + \chi_{112}^{(2)} E_1 E_2 + \chi_{113}^{(2)} E_1 E_3 + \chi_{121}^{(2)} E_2 E_1 + \chi_{122}^{(2)} E_2 E_2 \\ & + \chi_{123}^{(2)} E_2 E_3 + \chi_{131}^{(2)} E_3 E_1 + \chi_{132}^{(2)} E_3 E_2 + \chi_{133}^{(2)} E_3 E_3] \end{aligned} \quad (4.7)$$

indices were contracted by substituting Eqn.3.3 into Eqn.3.4

$$P_1 = \epsilon_0 [\chi_{11}^{(2)} E_1^2 + \chi_{12}^{(2)} E_2^2 + \chi_{13}^{(2)} E_3^2 + 2\chi_{14}^{(2)} E_2 E_3 + 2\chi_{15}^{(2)} E_1 E_3 + 2\chi_{16}^{(2)} E_1 E_2] \quad (4.8)$$

Then substitute Eqn.3.2 into Eqn.3.5

$$P_1 = 2\epsilon_0 [d_{11} E_1^2 + d_{12} E_2^2 + d_{13} E_3^2 + 2d_{14} E_2 E_3 + 2d_{15} E_1 E_3 + 2d_{16} E_1 E_2] \quad (4.9)$$

Repeat the calculations above for P_2 and P_3 ,

$$P_2 = 2\epsilon_0 [d_{21} E_1^2 + d_{22} E_2^2 + d_{23} E_3^2 + 2d_{24} E_2 E_3 + 2d_{25} E_1 E_3 + 2d_{26} E_1 E_2] \quad (4.10)$$

$$P_3 = 2\epsilon_0[d_{31}E_1^2 + d_{32}E_2^2 + d_{33}E_3^2 + 2d_{34}E_2E_3 + 2d_{35}E_1E_3 + 2d_{36}E_1E_2] \quad (4.11)$$

The indices 1, 2 and 3 were considered as x, y and z respectively;

$$1 = x \qquad 2 = y \qquad 3 = z \quad (4.12)$$

Then the nonlinear polarization was expressed in the matrix form;

$$\begin{pmatrix} P_x \\ P_y \\ P_z \end{pmatrix} = 2\epsilon_0 \begin{pmatrix} d_{11} & d_{12} & d_{13} & d_{14} & d_{15} & d_{16} \\ d_{21} & d_{22} & d_{23} & d_{24} & d_{25} & d_{26} \\ d_{31} & d_{32} & d_{33} & d_{34} & d_{35} & d_{36} \end{pmatrix} \begin{pmatrix} E_x^2 \\ E_y^2 \\ E_z^2 \\ 2E_yE_z \\ 2E_zE_x \\ 2E_xE_y \end{pmatrix} \quad (4.13)$$

Eqn. 4.13 is the general expression for polarization in a generative crystal. d -matrix in this expression varies crystal to crystal. Further calculations are done for ZnTe crystal and the d - matrix for ZnTe crystal is given as;

$$\begin{pmatrix} 0 & 0 & 0 & d_{14} & 0 & 0 \\ 0 & 0 & 0 & 0 & d_{14} & 0 \\ 0 & 0 & 0 & 0 & 0 & d_{14} \end{pmatrix} \quad (4.14)$$

An incident electric field on the crystal creates polarization. In our case, to calculate the polarization, we considered an arbitrary incident E-field,

$$\vec{E}_0 = E_0 \begin{pmatrix} \sin \theta \cos \phi \\ \sin \theta \sin \phi \\ \cos \theta \end{pmatrix} \quad (4.15)$$

where θ is the polar angle and ϕ is the azimuthal angle. Then the nonlinear polarization for ZnTe becomes;

$$\begin{pmatrix} P_x \\ P_y \\ P_z \end{pmatrix} = 2\epsilon_0 d_{14} \begin{pmatrix} 0 & 0 & 0 & 1 & 0 & 0 \\ 0 & 0 & 0 & 0 & 1 & 0 \\ 0 & 0 & 0 & 0 & 0 & 1 \end{pmatrix} \begin{pmatrix} E_0^2 \sin^2 \theta \cos^2 \phi \\ E_0^2 \sin^2 \theta \sin^2 \phi \\ E_0^2 \cos^2 \theta \\ 2E_0^2 \sin \theta \cos \theta \sin \phi \\ 2E_0^2 \sin \theta \cos \theta \cos \phi \\ 2E_0^2 \sin^2 \theta \sin \phi \cos \phi \end{pmatrix} \quad (4.16)$$

$$\begin{pmatrix} P_x \\ P_y \\ P_z \end{pmatrix} = 4\epsilon_0 d_{14} E_0^2 \begin{pmatrix} \sin \theta \cos \theta \sin \phi \\ \sin \theta \cos \theta \cos \phi \\ \sin^2 \theta \sin \phi \cos \phi \end{pmatrix} \quad (4.17)$$

For known angles intensity of the THz radiation was calculated. In this case the maximum intensity obtained from ZnTe crystal was considered. The maximum intensity was observed when the phase matching condition is satisfied. This is true when the group velocity of the optical beam is equal to the phase velocity of the THz beam. In addition to that, if the optical wave and THz wave propagates collinearly in the crystal, then this condition is called collinear phase matching.

It is assumed that matching condition is satisfied. Then the radiated THz intensity (I_{THz}) is proportional to amplitude of the nonlinear polarization ($|P|^2$) that caused by the applied electric field.

$$I_{\text{THz}} \propto |P|^2 \quad (4.18)$$

In order to calculate I_{THz} first $|P|^2$ was computed from Eqn.4.14;

$$\begin{aligned} |P|^2 &= P_x^2 + P_y^2 + P_z^2 \\ &= 16\epsilon_0^2 d_{14}^2 E_0^4 [\sin^2 \theta \cos^2 \theta \sin^2 \phi + \sin^2 \theta \cos^2 \theta \cos^2 \phi + \sin^4 \theta \sin^2 \phi \cos^2 \phi] \\ &= 16\epsilon_0^2 d_{14}^2 E_0^4 (\sin^2 \theta) [\cos^2 \theta (\sin^2 \phi + \cos^2 \phi) + \sin^2 \theta \sin^2 \phi \cos^2 \phi] \\ &= 4\epsilon_0^2 d_{14}^2 E_0^4 \sin^2 \theta [4 \cos^2 \theta + \sin^2 \theta (2 \sin \phi \cos \phi)^2] \\ &= 4\epsilon_0^2 d_{14}^2 E_0^4 \sin^2 \theta [4 \cos^2 \theta + \sin^2 \theta \sin^2 2\phi] \end{aligned} \quad (4.19)$$

THz intensity can be expressed in terms of maximum THz intensity. Then first, calculate the angles which maximize the intensity. The angles that maximize the intensity can be determined by equating the first derivative of the intensity to zero.

$$\begin{aligned}
I_{THZ} \propto |P|^2 &= 4\epsilon_0^2 d_{14}^2 E_0^4 \sin^2 \theta [4 \cos^2 \theta + \sin^2 \theta \sin^2 2\phi] \\
I_{THZ}^{max} \rightarrow dI_{THZ} &= 0 \\
dI &= \frac{\partial I}{\partial \theta} d\theta + \frac{\partial I}{\partial \phi} d\phi = 0
\end{aligned} \tag{4.20}$$

First, the partial derivative of intensity with respect to azimuthal angle was considered as:

$$\begin{aligned}
\frac{\partial I}{\partial \phi} \propto \frac{\partial |P|^2}{\partial \phi} &= \frac{2(\sin 2\phi)(\cos 2\phi) 2}{\sin 4\phi} = 0 \\
\sin 4\phi = 0 &\Rightarrow \boxed{\phi = \frac{\pi}{4}, \frac{3\pi}{4}}
\end{aligned} \tag{4.21}$$

Thus, intensity is maximized in azimuthal angle for ZnTe crystal. This angle corresponds to {110} plane. This is why <110> cut ZnTe was used in the experiment. In order to maximize the polar component, first substitute the ϕ value and obtain intensity I'_{THZ} in terms of polar angle.

$$\begin{aligned}
I'_{THZ} &\propto 4\epsilon_0^2 d_{14}^2 E_0^4 \sin^2 \theta (4 \cos^2 \theta + \sin^2 \theta) \\
I'_{THZ} &\propto 4\epsilon_0^2 d_{14}^2 E_0^4 \left(\frac{4 \sin^2 \theta \cos^2 \theta}{\sin^2 2\theta} + \sin^4 \theta \right) \\
I'_{THZ} &\propto 4\epsilon_0^2 d_{14}^2 E_0^4 (\sin^2 2\theta + \sin^4 \theta)
\end{aligned} \tag{4.22}$$

Second, the partial derivative of intensity with respect to polar angle was considered as,

$$\begin{aligned}
\frac{\partial I}{\partial \theta} \propto \frac{\partial |P|^2}{\partial \theta} &= 2(\sin 2\theta)(\cos 2\theta)2 + 4 \sin^3 \theta \cos \theta = 0 \\
&= 2(\sin 2\theta)(\cos 2\theta)2 + 2 \sin^2 \theta \underbrace{2 \sin \theta \cos \theta}_{\sin 2\theta} \\
&= \sin 2\theta \left(\underbrace{2 \frac{\cos 2\theta}{\cos^2 \theta - \sin^2 \theta} + \sin^2 \theta}_{=0} \right) = 0 \\
&\Rightarrow 2(\cos^2 \theta - \sin^2 \theta) + \sin^2 \theta = 0 \\
&\Rightarrow 2 \cos^2 \theta - \sin^2 \theta = 0 \\
&\Rightarrow 2 \cos^2 \theta - (1 - \cos^2 \theta) = 0 \\
&\Rightarrow 2 \cos^2 \theta - 1 + \cos^2 \theta = 0 \\
&\Rightarrow 3 \cos^2 \theta = 1 \\
&\Rightarrow \cos^2 \theta = \frac{1}{3} \\
&\Rightarrow \cos \theta = \frac{1}{\sqrt{3}} \Rightarrow \boxed{\theta = 54.7^\circ} \tag{4.23}
\end{aligned}$$

Then, the maximum intensity I_{THz}^{\max} at $\phi = \frac{\pi}{4}$ and at $\theta = 54.7$ can be calculated as,

$$\begin{aligned}
I_{THz}^{\max} &\propto 4\epsilon_0^2 d_{14}^2 E_0^4 \left(\frac{\sqrt{2}}{\sqrt{3}} \right)^2 \left(4 * \frac{1}{3} + \frac{2}{3} \right) \\
I_{THz}^{\max} &\propto \frac{16}{3} \epsilon_0^2 d_{14}^2 E_0^4 \tag{4.24}
\end{aligned}$$

From the ratio I'_{THz} and I_{THz}^{\max} THz intensity can be expressed in terms of θ .

$$\begin{aligned}
\frac{I'_{THz}}{I_{THz}^{\max}} &\propto \frac{4\epsilon_0^2 d_{14}^2 E_0^4 \sin^2 \theta (4 \cos^2 \theta + \sin^2 \theta)}{\frac{16}{3} \epsilon_0^2 d_{14}^2 E_0^4} \\
I_{THz}(\theta) &= \frac{3}{4} I_{THz}^{\max} \sin^2 \theta \left(4 \underbrace{\cos^2 \theta}_{1 - \sin^2 \theta} + \sin^2 \theta \right) \\
\boxed{I_{THz}(\theta) = \frac{3}{4} I_{THz}^{\max} \sin^2 \theta (4 - 3 \sin^2 \theta)} &\tag{4.25}
\end{aligned}$$

On the other hand, electric field of THz radiation is proportional to the polarization. Similarly, electric field of THz radiation can be calculated.

$$\vec{E}_{THz}(\theta, \phi) \propto \vec{P} = 4\epsilon_0 d_{14} E_0^2 \sin \theta \begin{pmatrix} \cos \theta \sin \phi \\ \cos \theta \cos \phi \\ \sin \theta \sin \phi \cos \phi \end{pmatrix} \quad (4.26)$$

Also electric field of THz radiation is proportional to magnitude of the polarization

$$E_{THz} = |\vec{E}_{THz}| \propto |\vec{P}| \quad (4.27)$$

In order to calculate the THz electric field, first compute the magnitude of the nonlinear polarization.

$$\begin{aligned} |P| &= \sqrt{P_x^2 + P_y^2 + P_z^2} \\ &= 4\epsilon_0 d_{14} E_0^2 \sin \theta \sqrt{\cos^2 \theta \sin^2 \phi + \cos^2 \theta \cos^2 \phi + \sin^2 \theta \sin^2 \phi \cos^2 \phi} \\ &= 4\epsilon_0 d_{14} E_0^2 \sin \theta \sqrt{\cos^2 \theta (\sin^2 \phi + \cos^2 \phi) + \sin^2 \theta \sin^2 \phi \cos^2 \phi} \\ &= 4\epsilon_0 d_{14} E_0^2 \sin \theta \sqrt{\cos^2 \theta + \sin^2 \theta \sin^2 \phi \cos^2 \phi} \end{aligned} \quad (4.28)$$

Then E_{THz} becomes,

$$E_{THz} \propto |\vec{P}| = 4\epsilon_0 d_{14} E_0^2 \sin \theta \sqrt{\cos^2 \theta + \sin^2 \theta \sin^2 \phi \cos^2 \phi} \quad (4.29)$$

Electric field of THz radiation (E_{THz}) can also be expressed in terms of maximum electric field (E_{THz}^{\max}) and the polar angle (θ). The angles that maximize the intensity are also the same angles that maximize the electric field. Thus, as to evaluate E_{THz} , E_{THz}^{\max} was calculated first, than polar angle dependent electric field $E'_{THz}(\theta)$ was computed by inserting the $\phi = 3\pi/4$ value into the Eqn. 4.26. Then electric field of THz radiation E_{THz} was expressed in terms of maximum radiated THz electric field E_{THz}^{\max} .

Maximum intensity occurs at the angles defined below;

$$\phi = \frac{3\pi}{4} \text{ and } \theta = 54.7, \left(\sin \theta = \frac{\sqrt{2}}{\sqrt{3}}, \cos \theta = \frac{1}{\sqrt{3}} \right)$$

Then E_{THz}^{max} can be calculated as;

$$\begin{aligned}
E_{THz}^{max} &\propto 4\epsilon_0 d_{14} E_0^2 \frac{\sqrt{2}}{\sqrt{3}} \sqrt{\frac{1}{3} + \frac{2}{3} \frac{1}{2} \frac{1}{2}} \\
E_{THz}^{max} &\propto 4\epsilon_0 d_{14} E_0^2 \frac{\sqrt{2}}{\sqrt{3}} \sqrt{\frac{3}{6}} \\
E_{THz}^{max} &\propto \frac{4}{\sqrt{3}} \epsilon_0 d_{14} E_0^2
\end{aligned} \tag{4.30}$$

The electric field that depends only on polar angle ($E'_{THz}(\theta)$) can be evaluated by substituting the value of azimuthal angle that maximizes the electric field at that angle,

$$\vec{E}'_{THz}(\theta) \propto 4\epsilon_0 d_{14} E_0^2 \sin \theta \begin{pmatrix} \frac{2}{\sqrt{2}} \cos \theta \\ -\frac{2}{\sqrt{2}} \cos \theta \\ -\frac{1}{2} \sin \theta \end{pmatrix} \tag{4.31}$$

The ratio of the Eqn. 4.31 to Eqn. 4.30 is:

$$\frac{\vec{E}'_{THz}(\theta)}{E_{THz}^{max}} \propto \frac{2\epsilon_0 d_{14} E_0^2 \sin \theta \begin{pmatrix} \sqrt{2} \cos \theta \\ -\sqrt{2} \cos \theta \\ -\sin \theta \end{pmatrix}}{\frac{4}{\sqrt{3}} \epsilon_0 d_{14} E_0^2} \tag{4.32}$$

Then, electric field of the radiated THz becomes:

$$\boxed{\vec{E}_{THz}(\theta) = \frac{\sqrt{3}}{2} E_{THz}^{max} \sin \theta \begin{pmatrix} \sqrt{2} \cos \theta \\ -\sqrt{2} \cos \theta \\ -\sin \theta \end{pmatrix}} \tag{4.33}$$

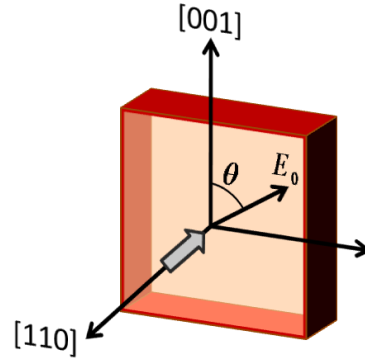


Figure 4.5 Crystal Orientation according to the incoming electric field (E_0)

In the Figure 4.5 ZnTe crystal orientation is seen according to an arbitrary incoming electric field (E_0). The direction of propagation of the incoming electric field is indicated with the gray arrow. The angle θ is the polar angle. And this angle based on our calculation above is 54.7 degrees.

4.3 CRYSTAL DETECTION

In this technique, the same crystals are used as detector. Electro optic sampling uses the same principles with the optical rectification. As mentioned in the *Section 1.1.2 Optical Rectification for Generation*, optical and THz pulses propagate in the crystal with different velocities. This velocity mismatch can be tolerated over a distance. This distance is called coherent length (See Figure 4.6).

$$l_c = \frac{c}{2v_{THZ}|n_{gr}-n_T|} \quad (4.34)$$

where,

$$n_{gr}(\lambda) = n_o(\lambda) - \lambda \frac{\partial n_o}{\partial \lambda} \quad (4.35)$$

ω_{THz} is the THz frequency, n_{gr} is optical group refractive index, n_T is THz refractive index (Eqn. 2.5) and n_o is the optical refractive index of the crystal (Eqn. 2.4) [1].

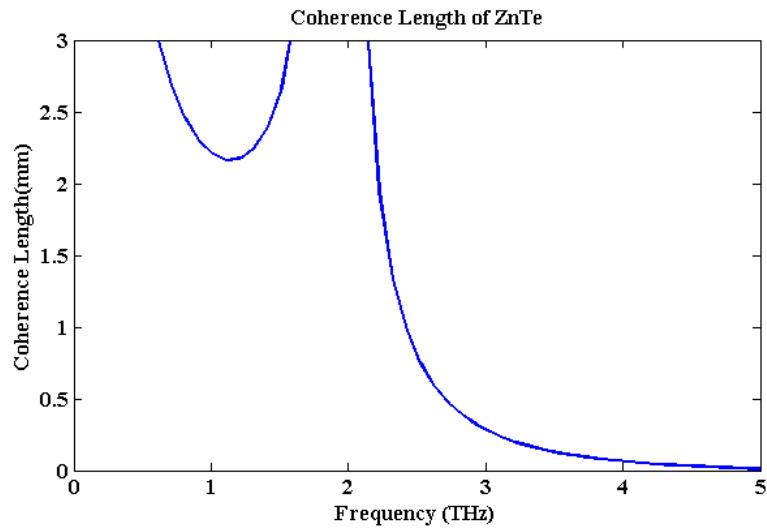


Figure 4.6 Coherent length of ZnTe crystal.

THz and the optical pulse focused on the crystal and propagate collinearly in the crystal. If the phase-mismatch condition is satisfied, then the existence of the THz beam causes birefringence, which is the change of the refractive index along the axes of the crystal. When the linearly polarized optical pulse passes through the crystal, it detects the difference in the refractive index of the axes and hence the polarization changes. This causes a change in its polarization.

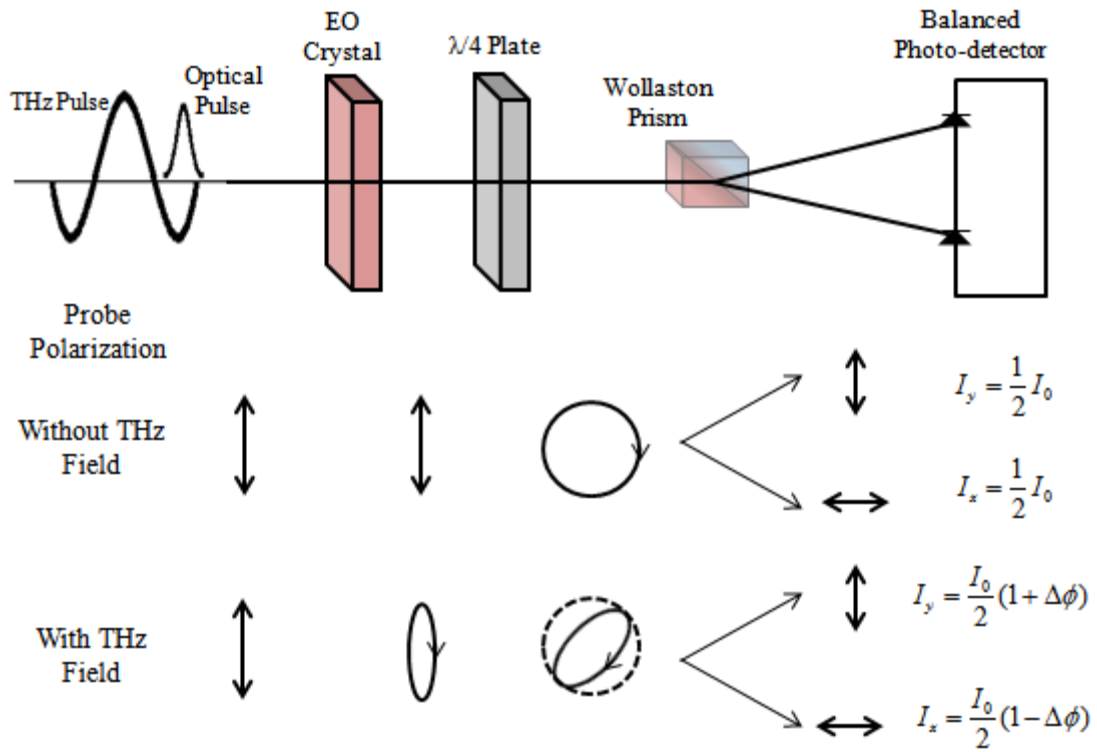


Figure 4.7 Schematic representation of EO crystal detection

A schematic representation is seen in the Figure 4.7 In order to measure the polarization difference wave plate; Wollaston prism and a photo detector are used, respectively. After the crystal optical beam passes wave plate and changes polarization. When the THz beam is incident on the crystal then the wave plate polarization will be changed. Wollaston prism separates the circularly polarized light into its components.

In the case, where the THz is present due to phase delay, photo detector senses the difference between the components of the polarized light. This delay is also called phase retardation and proportional to THz electric field E_{THz} , crystal thickness l , linear EO coefficient of the crystal r_{14} , refractive index of the crystal at optical frequency n_o and the optical wavelength λ [28].

$$\Gamma \propto \frac{1}{\lambda} l n_o^3 r_{14} E_{THz} \quad (4.36)$$

The results show that maximum signal detection is obtained when the THz pulse polarization and probe beam pulse polarization are parallel or orthogonal to each other [47].

4.4 Results of Crystal - Crystal THz system

In the crystal – crystal THz system different focusing lenses were used in the THz generation. Also different off axis parabolic mirrors (OAPM) were used in the system. Different focusing lenses affected the THz peak to peak value. The results are shown in the Table 4.1.

Table 4.1 THz peak values with different lens of changing focal length

Focal length of OAPM	Focal Length of Lens	THz Peak-Peak
120 mm	50 mm	2,027mV
120 mm	75 mm	2,154 mV
120 mm	100 mm	2,243 mV

The results show that, the focal length of lens and the focal length of the off-axis parabolic mirrors should be confocal.

Table 4.2 Comparison of the power spectrum for the different crystal-crystal systems

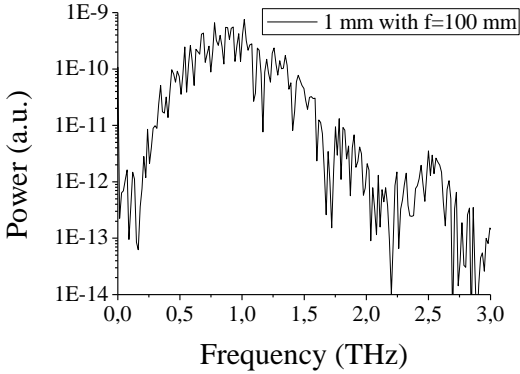
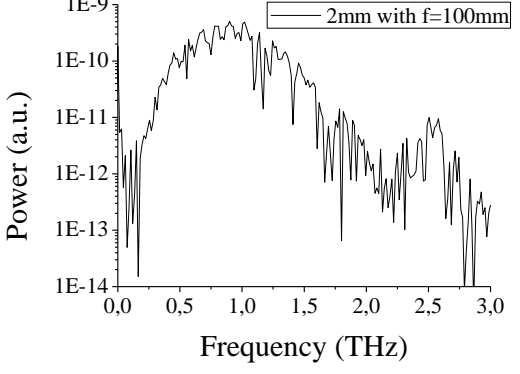
D. Crystal Thickness	Focal Length	OAPM Focal Length	Power Spectrum
1mm	f=100 mm Lens	120mm	
2mm	f=100 mm Lens	120mm	

Table 4.2 shows the power spectrum of the system with respect to the changing focal length of the focusing lens. In this system chopper frequency was set to 2.5 kHz. Data was obtained with balanced photodiode in medium sensitivity. If we consider the both cases, power spectrum shows ~2 THz bandwidth. 2 mm crystal thickness gives better signal-to-noise ratio.

Table 4.3 Comparison of the power spectrum for different OAPM Focal Length

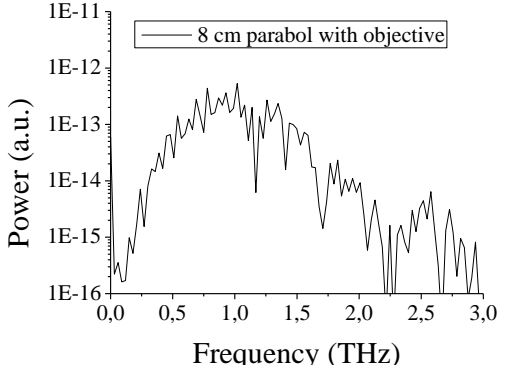
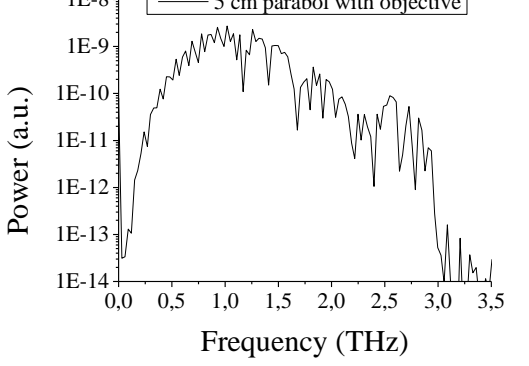
D. Crystal Thickness	Magnification	OAPM Focal Length	Power Spectrum
2mm	2.5x objective (~30 mm focal length)	80mm	
2mm	2.5x objective (~30 mm focal length)	50mm	

Table 4.3 shows the power spectrum of the system. Focusing component was used as 2.5x Melles Griot objective. The chopper frequency was set to 250 Hz. In the system collimator parabolic mirror was changed. Different focal lengths were compared. Spectrum of the first system has ~2.2 THz bandwidth; however the other system has ~3 THz bandwidth. A lens with 50 mm focal length was compared with parabolic mirror with 50 mm focal length. The results were not different from the result with the 2.5x objective.

CHAPTER 5

CONCLUSION

In this study two different THz Time Domain Spectroscopy (THz-TDS) systems were developed. In one of them, THz generation was done by a photoconductive antenna. In the other system THz generation was done by an electro-optic crystal. In both of these systems electro-optic detection was used as a detection method. In chapter one the development of THz studies was covered. Generation and detection techniques for THz system were discussed in chapter two. Then in chapter three, an antenna-crystal system was described with a sample analysis in the system. Different samples such as selenium and vitamin B₁₂ were analyzed in the antenna-crystal system. Experimental results showed that, broader spectral frequency was necessary for absorption analysis. Different materials give different spectral peaks at high frequencies. More spectral information can be obtained for higher frequencies. In addition, sample thickness was found to be a limitation in bandwidth obtained.

To obtain higher frequencies crystal generation and crystal detection THz-TDS system was constructed and discussed in chapter 4. The problem with this system is that since our laser source is nanojoule energy per pulse ultrafast laser (non-amplified laser); the signal to noise ratio is very low. Typically people who use crystal for non-linear THz generation use high peak power laser sources to obtain better signal to noise ratios. In order to overcome this limitation we analyzed the best possible configuration we can achieve with a THz-TDS system driven by a nanojoule energy per pulse ultrafast laser (non-amplified laser) source which uses a ZnTe

crystal for non-linear generation of THz radiation. To maximize the generated power a description of the well-documented theory of crystal generation was given. Calculations of radiated THz intensity and electric field were derived for ZnTe crystal. It was found that the best possible orientation of the $\langle 110 \rangle$ ZnTe crystal was when its crystal axis $\langle 100 \rangle$ axis made an angle of 54.7 degrees with the linear polarization of the pump beam from our nanojoule energy per pulse ultrafast laser (non-amplified laser) source. Electro-optic detection was also explained briefly in this chapter and optimal configuration was discussed. We also showed that to obtain higher frequencies we need thinner crystals. This was explained in terms of walk off length in generation and coherence length in detection of THz pulses. It was shown that for very short pulses we need very thin crystals to see larger THz frequencies. However as the crystal thickness decreases THz generation power decreases as well due to lower efficiencies. Different crystal thicknesses were tried in detection but it was not successful to have a broader spectrum. This was due to the fact that to obtain a much broader spectrum we needed a high peak power laser source with a thin crystal for generation. Also different thicknesses were tried in detection but again since our generated frequency spectrum was narrow we could not see the higher frequencies. If we had generated high frequencies with sufficient power then we would need a crystal that is thinner than the crystal thickness that we used for detection. In addition ZnTe crystals sometimes have defects inside, a result of the manufacture process, which can be considered as defects. Thus the largest bandwidth we were able to achieve was 3 THz.

In order to improve the signal to noise ratio of our system we tried to also optimize the optical components which guide the THz beam in the THz-TDS system. When we improve the signal to noise we also improved our detection bandwidth. We used different focal length lenses/objectives as well as different focal length parabolic mirrors to generate and collect the THz radiation. Results showed that it is important that the focal length of the focusing lens and the focal length of the collimating parabolic reflectors have equal focal lengths.

THz-TDS systems were constructed to analyze various samples. Optimized systems were built in spite of the difficulties in the alignment. An advantage of the sample

analysis in these systems is that the ability of directly calculating absorption coefficient and refractive index of the sample. However, a spectroscopy having broader bandwidth is not easy to obtain. In our case, THz system up to 1 THz was obtained with photoconductive antenna generation. Another system with broader bandwidth up to 3 THz was expanded by optical rectification. Higher frequencies could not be reached due to crystal thicknesses. Since the EO sampling method does not depend on material properties such as carrier recombination time, a broader spectrum could be reached with different pump laser having different repetition time.

In conclusion, THz-TDS system was built with two different generation methods. In the antenna-crystal system absorption coefficient and real refractive indices of the various samples were calculated. Crystal-crystal system was built with a broader spectrum. Theoretical calculation of radiated intensity and electric field was done for crystal generation. Best parameters for crystal generation were found with nanojoule energy per pulse ultrafast laser (non-amplified laser) system.

REFERENCES

- [1] Y. S. Lee “ Principles of Terahertz Science and Technology” *Springer Science+Business Media, LLC*, (2009)
- [2] I. Jones, T. J. Rainsford, B. Fischer and D. Abbott “ Towards T-ray spectroscopy of retinal isomers: A review of methods and modelling” *Vibrational Spectroscopy* **41**, 144-154 (2006)
- [3] X.C. Zhang, and J. Xu, “Introduction to THz Wave Photonics” *Springer Science+Business Media, LLC*, (2010)
- [4] K. Sakai, and M. Tani, “Introduction to Terahertz Pulses” *K. Sakai (Ed.): Terahertz Optoelectronics, Topics Appl. Phys.*, **97**, 1-30 (2005)
- [5] D. F. Plusquellic, K. Siegrist, E. J. Heilweil, and O. Esenturk “Applications of Terahertz Spectroscopy in Biosystems” *Chem. Phys. Chem.* **8**, 2412-2431 (2007)
- [6] Y. Ung, B. M. Fischer, H. Ng and D. Abbott “Towards Quality Control of Food Using Terahertz” *Proc. of SPIE* **6799** (2007)
- [7] D. H. Auston “Picosecond optoelectronic switching and gating in silicon” *Appl. Phys. Lett.* **26**, 3, 101-103 (1975)
- [8] Chi H. Lee “Picosecond optoelectronic switching in GaAs” *Appl. Phys. Lett.* **30**, 2, 84-86 (1977)
- [9] G. Mourou, C. V. Stancampiano, A. Antonetti, and A. Orszag “Picosecond microwave pulses generated with a subpicosecond laser-driven semiconductor switch” **39**, 4, 295-296 (1981)
- [10] R. Heidemann, Th. Pfeiffer, D. Jäger, “Optoelectronically pulsed slot-line antennas” *Electron. Lett.* **19**, 9, 316-317 (1983)

- [11] P. R. Smith, D. H. Auston, and M. C. Nuss, “Subpicosecond Photoconducting Dipole Antennas” *IEEE J. Quantum. Electron.* **24**, 2, 255-260 (1988)
- [12] M. V. Exter, Ch. Fattering, and D. Grischkowsky, “High-brightness terahertz beams characterized with an ultrafast detector” *Appl. Phys. Lett.* **55**, 4, 337-339 (1989)
- [13] S. Matsuura, and H. Ito, “Generation of CW Terahertz Radiation with Photomixing” *K. Sakai (Ed.): Terahertz Optoelectronics, Topics Appl. Phys.*, **97**, 157-202 (2005)
- [14] M. Bass, P. A. Franken, J. F. Ward, and G. Weinreich “Optical rectification” *Phys. Rev. Lett.* **9**, 11, 446–448 (1962)
- [15] T. Yajima and N. Takeuchi “Spectral Properties and Tunability of Far-Infrared Difference-Frequency Radiation Produced by Picosecond Laser Pulses” *Jpn. J. Appl. Phys.* **10**, 907-915 (1971)
- [16] K. H. Yang, P. L. Richards, and Y. R. Shen “Generation of Far-Infrared Radiation by Picosecond Light Pulses in LiNbO₃” *Appl. Phys. Lett.* **19**, 9, 320-323 (1971)
- [17] X.-C. Zhang, B. B. Hu, J. T. Darrow, and D. H. Auston “Generation of femtosecond electromagnetic pulses from semiconductor surfaces” *Appl. Phys. Lett.* **56**, 11, 1011-1013 (1990)
- [18] B. B. Hu, X.-C. Zhang, and D. H. Auston “Temperature dependence of femtosecond electromagnetic radiation from semiconductor surfaces” *Appl. Phys. Lett.* **57**, 25, 2629-2631 (1990)
- [19] K. Leo, J. Shah, E. O. Göbel, T. C. Damen, S. Schmitt-Rink, W. Schäfer and K. Köhler “Coherent oscillations of a wave packet in a semiconductor double-quantum-well structure” *Phys. Rev. Lett.* **66**, 2, 201-204 (1991)
- [20] G. P. Williams, “Far-IR/THz radiation from the Jefferson Laboratory, energy recovered linac, free electron laser,” *Rev. Sci. Instrum.* **73**, 3, 1461–1463 (2002)

- [21] T. Dekorsy, H. Auer, C. Waschke, H.J. Bakker, H.G. Roskos, H. Kurz, V. Wagner, and P. Grosse “Emission of submillimeter electromagnetic waves by coherent phonons” *Phys. Rev. Lett.* **74**, 5, 738-741 (1995)
- [22] R. Kersting, K. Unterrainer, G. Strasser, H. F. Kauffmann, and E. Gornik, “Few-Cycle THz Emission from Cold Plasma Oscillations” *Phys. Rev. Lett.* **79**, 16, 3038-3041 (1997)
- [23] M. Hangyo, S. Tomozawa, Y. Murakami, M. Tonouchi, M. Tani, Z. Wang, K. Sakai, and S. Nakashima “Terahertz radiation from superconducting $\text{YBa}_2\text{Cu}_3\text{O}_{7-\delta}$ thin films excited by femtosecond optical pulses” *Appl. Phys. Lett.* **69** 14, 2122-2124 (1996)
- [24] D. H. Auston and P. R. Smith “Generation and detection of millimeter waves by picosecond photoconductivity” *Appl. Phys. Lett.* **43**, 7, 631-633 (1983)
- [25] D. H. Auston, K. P. Cheung, and P. R. Smith, “Picosecond photoconducting Hertzian dipoles” *Appl. Phys. Lett.* **45**, 3, 284-286 (1984)
- [26] D. H. Auston, K. P. Cheung, J. A. Valdmanis, and D. A. Kleinman “Cherenkov Radiation from Femtosecond Optical Pulses in Electro-Optic Media” *Phys. Rev. Lett.* **53**, 16, 1555-1558 (1984)
- [27] J. C. Wiltse, “History of millimeter and submillimeter waves” *IEEE Trans. On Microwave Theo. and Thec.* **32**, 9 (1984)
- [28] S. L. Dexheimer, “Terahertz Spectroscopy: Principles and Applications” *CRC Press*, (2008)
- [29] Z. Zhang, Y. Zhang, G. Zhao and C. Zhang, “ Terahertz time-domain spectroscopy for explosive imaging” *Optik*, **118**, 325-329 (2007)
- [30] W. L. Chan, J. D. Deibel and D. M. Mittleman, “ Imaging with Terahertz Radiation” *Rep. Prog. Phys.* **70**, 1325-1379 (2007)
- [31] B. B. Hu and M. C. Nuss, “Imaging with terahertz waves” *Opt. Lett.* **20**, 16, 1716-1718 (1995)

- [32] N. Kida, H. Murakami and M. Tonouchi, "Terahertz Optics in Strongly Correlated Electron Systems" *K. Sakai (Ed.): Terahertz Optoelectronics, Topics Appl. Phys.*, **97**, 271-330 (2005)
- [33] Y. Konishi, M. Kamegawa, M. Case, R. Yu, M. J. W. Rodwell, R. A. York, and D. B. Rutledge, "Picosecond electrical spectroscopy using monolithic GaAs circuits" *Appl. Phys. Lett.* **61**, 23, 2829-2831 (1992)
- [34] A. Nahata, A. S. Weling, and T. F. Heinz, "A wideband coherent terahertz spectroscopy system using optical rectification and electro-optic sampling" *Appl. Phys. Lett.* **69**, 16, 2321-2323 (1996)
- [35] Q. Wu, and X.-C. Zhang, "Design and characterization of traveling-wave electrooptic terahertz sensors," *IEEE J. Select. Top. Quantum. Electron.* **2**, 693 (1996)
- [36] G. Gallot and D. Grischkowsky, "Electro-optic detection of terahertz radiation," *J. Opt. Soc. Am.* **16**, 8, 1204-1212 (1999)
- [37] Q. Wu and X.-C. Zhang, "Free-space electro-optic sampling of terahertz beams" *Appl. Phys. Lett.* **67**, 24, 3523- 3525 (1995)
- [38] A. Nahata and H. Cao, "Broadband phase-matched generation and detection of terahertz radiation" *Proceedings of SPIE* **5411**, 150-157 (2004)
- [39] A. Nahata, D. H. Auston, T. F. Heinz and C. Wu, "Coherent detection of freely propagating terahertz radiation by electro-optic sampling" *Appl. Phys. Lett.* **68**, 8, 150-152 (1996)
- [40] Thorlabs, <http://www.thorlabs.com/catalogpages/v20/706.pdf>, last visited 10/01/2011
- [41] Batop, http://www.batop.de/products/photoconductive-antenna/data-sheet/manual_PCA-44-06-10-1030.pdf, last visited 10/01/2011

- [42] CVI Melles Griot, <http://www.cvimellesgriot.com/Products/Documents/Catalog/POA.pdf>, last visited 10/01/2011
- [43] Stanford Research Systems, <http://www.thinksrs.com/downloads/PDFs/Manuals/SR830m.pdf>, last visited 10/01/2011
- [44] TYDEX, http://www.tydexoptics.com/pdf/THz_Materials.pdf, last visited 10/01/2011
- [45] C. A. Schmuttenmaer, “ Exploring Dynamics in the Far-Infrared with Terahertz Spectroscopy” *Chem. Rev.* **2004**, 104, 1759-1779 (2003)
- [46] Y.-S. Lee, T. Meade, V. Perlin, H. Winful, and T. B. Norris, “ Generation of narrow-band terahertz radiation via optical rectification of femtosecond pulses in periodically poled lithium niobate” *Appl. Phys. Lett* **76**, 18, 2505-2507 (2000)
- [47] P. C. M. Planken, H.-K. Nienhuys, H. J. Bakker and T. Wenckebach “Measurement and calculation of the orientation dependence of terahertz pulse detection in ZnTe” *J. Opt. Soc. Am. B* **18**, 3, 313-317 (2001)